DOI:
10.1002/chem.201701939

Document Version
Peer reviewed version

Cancer Stem Cell and Bulk Cancer Cell Active Copper(II) Complexes with Vanillin Schiff Base Derivatives and Naproxen

Chunxin Lu,[a] Arvin Eskandari,[a] Paul B. Cressey,[a] and Kogularamanan Suntharalingam*[a]

Dedication ((optional))

Abstract: Four copper(II) complexes, **1**-**4** containing regioisomeric vanillin Schiff base derivatives ((E)-5/4/3/2-methoxy-2-(((2-(methylthio)ethyl)imino)methyl)phenol) and the nonsteroidal anti-inflammatory drug (NSAID), naproxen, were synthesised and characterised. All complexes effectively cleave DNA in cell-free systems, with **4** displaying the highest nuclease activity. DNA binding studies suggest that **4** binds to DNA via the grooves prior to inducing oxidative DNA cleavage. Three of the complexes (**1**, **3**, and **4**) indiscriminately kill cancer stem cell (CSC)-enriched cells (HMLER-shEcad) and bulk cancer cells (HMLER) at micromolar concentrations. The most effective complex, **4** also reduced the formation and size of mammospheres to a similar extent as salinomycin, a well-established CSC-potent agent. Mechanistic studies show that **4** is readily taken up by CSCs, elevates intracellular reactive oxygen species (ROS) levels, causes DNA damage, and induces caspase-dependent apoptosis. Furthermore, **4** inhibits cyclooxygenase-2 (COX-2) expression and causes COX-2-dependent CSC death. The advantage of **4** over bulk cancer cell- or CSC-selective agents is that it has the potential to remove whole tumor populations (bulk cancer cells and CSCs) with a single dose.

Tumors are made up of complex heterogenous cancer cell populations with hierarchical organization.[1] Cancer stem cells (CSCs) are a small, biological distinct subset within the total malignant cell population perched atop the tumor hierarchy.[2] Like normal stem cell, CSCs are immortal or long-lived and thus have the potential to accumulate the necessary mutations for malignant transformation and subsequent tumor initiation.[3] CSCs are also linked to metastasis due to their unlimited tumor-initiating potential and inherent plasticity to survive secondary tumor sites.[4] Given the evolutionary predisposition of stem cells to survive harsh conditions, CSCs can escape attack from current chemotherapeutic and radiation regimens (at their therapeutically administered doses).[5] Several mechanisms potentially contribute to CSC chemo- and radio-resistance, these include; overexpression of quiescence CSCs that can evade treatments targeting proliferative cells, overactivation of multiple developmental signalling pathways, upregulation of anti-apoptotic proteins combined with the downregulation of pro-apoptotic machinery, and increased capacity for DNA repair.[6] The clinical implication of CSCs is that elimination of entire tumor populations, including CSCs, is necessary for long-lasting outcomes, and the failure to do so leaves open the possibility of cancer reoccurrence. Although a great amount of time has been devoted to identifying CSC therapeutic targets such as cell surface markers, organelles, dysregulated signalling pathways, and components of their microenvironment,[7] there is still no clinically approved agent (chemical or biological) that can simultaneously remove bulk cancer cells and CSCs. The development of CSC-potent agents is in its early stage and most of the drug candidates undergoing pre-clinical or clinical trials are completely organic in nature. We and others have recently shown that metal-containing compounds are also capable of potently killing CSCs and bulk cancer cells.[8]

CSCs maintain relatively low levels of reactive oxygen species (ROS) compared to bulk cancer cells.[9] The low ROS concentration in CSCs is associated to increased expression of free radical scavenging systems. This protects CSCs from biomolecule damage and contributes to chemo- and radio-resistance. As CSCs have adapted to thrive in ROS-deficient conditions, the intracellular redox state in CSCs is thought to be finely regulated. Therefore, the application of ROS-inducer, in tandem with CSC-targeted therapies, represents a potentially efficacious strategy for eradicating CSCs. Using this approach, we previously developed a series of copper(II)-phenanthroline complexes containing the nonsteroidal anti-inflammatory drugs (NSAID); indomethacin, naproxen, and tolfenamic acid, capable of selectivity killing breast CSCs over bulk breast cancer cells.[8b,8e] The copper(II)-phenanthroline-NSAIDs complexes induced CSC death by increasing intracellular ROS levels and inhibiting cyclooxygenase-2 (COX-2), an enzyme that catalyzes the rate-limiting step of prostaglandin biosynthesis (from arachidonic acid). COX-2 is involved in inflammatory response, linked to cancer progression and dissemination, and promotes stem cell renewal and proliferation.[10]

As CSC-specific agents only target a small subpopulation of tumor cells, they cannot rapidly reduce tumor mass when administered alone.[11] Thus, CSC-specific agents cannot provide the short term, measurable readout typically required for successful clinical trials. Removing CSCs using CSC-specific agents will, however, inhibit tumor growth over the longer term as CSCs will no longer be present to replenish the bulk tumor population.[11] Given the current methodologies used to evaluate the clinical efficacy of anticancer therapies, the most effective and measurable cancer treatments (in the short and long term) are those that can concurrently reduce tumor bulk and kill CSCs. Here, we present a series copper(II) complexes with regioisomeric vanillin Schiff base derivatives and naproxen, **1**-**4**. Three of the complexes (**1**, **3**, and **4**) effective kill CSCs and bulk cancer cells within a small concentration window. The mechanism of action of the most effective complex in the series, **4** is described in detail. Schiff base copper(II) complexes are well-known ROS generators capable of inducing apoptosis in various cancer cells by DNA damage or mitochondrial

[a] Dr K. Suntharalingam, Dr. C. Lu, P.B. Cressey, Arvin Eskandari
Department of Chemistry
King's College London
London
SE1 1DB, UK
E-mail: kogularamanan.suntharalingam@kcl.ac.uk

Supporting information for this article is given via a link at the end of the document.

dysfunction,[12] however, there have been no reports on their CSC activity.

Results and Discussion

Synthesis and Characterization

The copper(II) complexes, **1**-**4** were synthesized as outlined in Scheme 1. The vanillin Schiff base ligands, **L$^{1-4}$** were prepared by refluxing equimolar amounts of 2-(methylthio)ethan-1-amine with the appropriate 2-hydroxy-methoxybenzaldehyde in ethanol for 16 h. The ligands, **L$^{1-4}$** were isolated in good yields (90-95%) as yellow oils and fully characterized by ^{1}H and ^{13}C NMR, infrared spectroscopy, and API-MS mass spectrometry (see ESI). Characteristic signals at 8.23-8.83 ppm in the ^{1}H NMR spectra and C=N bands at 1622-1641 cm^{-1} in the IR spectra for **L$^{1-4}$** confirmed formation of the imine functionality. Disappearance for the aldehyde peak (*ca.* 9.90 ppm) associated to the various 2-hydroxy-methoxybenzaldehyde starting materials established full conversion. The copper(II) complexes, **1**-**4** were prepared by refluxing **L$^{1-4}$** with $Cu(NO_3)_2{\cdot}3H_2O$ and naproxen in ethanol (pH 7, adjusted by triethylamine) for 24 h. The complexes were isolated in reasonable yields (20-67%) as green solids and characterized by high-resolution ESI-TOF mass spectrometry, infrared spectroscopy, and elemental analysis (see ESI). Distinctive molecular ion peaks corresponding to the reduced forms of **1**-**4** with the appropriate isotopic pattern were observed in the ESI-TOF mass spectra (*m/z* = 519.0647 a.m.u, [reduced **1**+H]$^{+}$; 519.0680 a.m.u. [reduced **2**+H]$^{+}$; 519.0668 a.m.u. [reduced **3**+H]$^{+}$; 519.0692 a.m.u. [reduced **4**+H]$^{+}$) (Figure S1-4). The IR spectra for **1**-**4** displayed $\nu_{asym}(CO_2)$ and $\nu_{sym}(CO_2)$ stretching bands at 1602-1609 cm^{-1} and 1384-1397 cm^{-1}, respectively (Figure S5). The difference, Δ, between the $\nu_{asym}(CO_2)$ and $\nu_{sym}(CO_2)$ stretching bands for **1**-**4** varied between 205-225 cm^{-1}, suggestive of an unidentate coordination mode for the carboxylate moiety on naproxen to the copper center.[13] This assignment is consistent with that reported for other copper(II) complexes bearing tridentate Schiff bases and carboxylic acid-containing ligands.[14] The purity of **1**-**4** was established by elemental analysis.

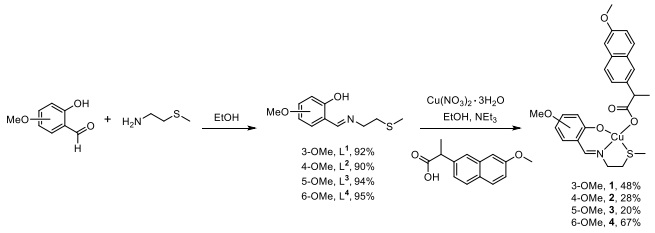

Scheme 1. The reaction scheme for the preparation of the vanillin Schiff base ligands, **L$^{1-4}$** and the corresponding copper(II) complexes, **1**-**4**.

DNA Cleavage and Binding Studies

Several Schiff base copper(II) complexes have been reported to bind and cleave double stranded DNA.[12] The DNA nuclease activity of **1**-**4** was assessed by agarose gel electrophoresis. Upon incubation of plasmid pUC19 DNA (100 ng) with **1**-**4** (0–50 μM for 24 h in the absence of external reducing agents), a marked decrease in the amount of supercoiled DNA (form I) and a concurrent increase in the amount of nicked circular DNA (form II) was observed, indicative of DNA cleavage (Figure 1A and S6). Complexes **2** and **4** displayed the highest nuclease activity with complete conversion of supercoiled to nicked circular DNA occurring at 10 μM. In the presence of ascorbic acid, **4** induced complete conversion of supercoiled DNA (form I) to circular and linear DNA (form II/III) at 10 μM, and cleavage into several small fragments at higher concentrations (25-50 μM) (Figure 1B). The enhanced nuclease activity of **4** in the presence of ascorbic acid, suggests that **4**-mediated DNA cleavage is redox-dependent. To determine the oxidative mechanism by which **4** induces DNA cleavage, nuclease activity was probed in the presence of reactive oxygen species (ROS) scavengers (NaN_3, KI, DMSO, and ^{t}BuOH) (Figure 1C). KI and NaN_3 displayed the greatest inhibitory effect, suggesting that hydrogen peroxide (H_2O_2) and singlet oxygen ($^{1}O_2$) are the major ROS intermediates formed during the DNA cleavage process. We propose that the copper(II) complex undergoes reduction to the corresponding copper(I) form by guanine bases in pUC19 DNA. The copper(I) form then reduces molecular oxygen to superoxide, which generates hydrogen peroxide.[15] The paramagnetic copper(II) form and the naproxen moiety could be responsible for singlet oxygen generation, via a photo-redox pathway in ambient light.[14b,16] To shed light on the DNA-binding mode of **4** prior to initiating DNA cleavage, the nuclease activity was probed in the presence of a minor groove binder (DAPI, 2-(4-amidinophenyl)-1H-indole-6-carboxamidine, 50 μM) and a major groove binder (methyl green, 50 μM). DNA cleavage was inhibited in the presence of methyl green and DAPI, suggesting that **4** binds to both the minor and major DNA grooves (Figure 1D).

To elucidate the binding affinity and further investigate the binding mode of **4** to duplex DNA, UV-Vis spectroscopic titrations were performed. Upon addition of aliquots of calf thymus DNA (ct-DNA), in the mM range, to a solution of **4** (50 μM), significant spectral changes were observed (Figure 1E). The absorption band corresponding to the metal perturbed intra-ligand π-π* transition (298 nm) displayed hypochromicity (20.0 ± 0.2 %), and bathochromicity (10.0 ± 0.6 nm). Three sharp isosbestic points were also noted. These features are characteristic of interactions with DNA bases, either by intercalation or groove binding. From the absorbance, the concentration of bound and unbound **4** was calculated and extrapolated to determine the binding constant (see ESI, Figure S7).[17] The intrinsic binding affinity of **4** to ct-DNA was calculated to be 1.3 ± 0.3 × 10^{5} M^{-1}. This value is 1 to 2 orders of magnitude lower than those reported for strong metallointercalators,[18] suggesting that a non-intercalative binding interaction could be operative.

To examine the binding mode of **4** to DNA further, DAPI and ethidium bromide (a strong intercalator) displacement studies were performed. Upon incremental addition of **4** (0 - 200 μM) to a solution of ct-DNA (20 μM) and DAPI (1 μM), the emission associated to the DAPI-DNA complex (originating from the binding of DAPI to the minor groove) markedly decreased (Figure S8). In contrast, upon incremental addition of **4** (0 - 200 μM) to a solution of ct-DNA (20 μM) and ethidium bromide (1 μM), the emission associated to the ethidium bromide-DNA complex (originating from the intercalation of ethidium bromide

between DNA base pairs) was largely unaltered (Figure S9). This suggests that **4** preferentially binds to the DNA grooves (over intercalation). Control studies with naproxen and **L**^{4} revealed that naproxen (0 - 200 µM) does not effectively displace DAPI from ct-DNA (Figure S10), whereas **L**^{4} (0 - 200 µM) displaces DAPI to a similar extent as **4** (Figure S11), suggesting that the groove binding ability of **4** is facilitated by the **L**^{4} moiety. Collectively, the DNA cleavage, UV-Vis titration and dye displacement studies suggest that **4** binds to DNA via the grooves prior to inducing oxidative DNA cleavage.

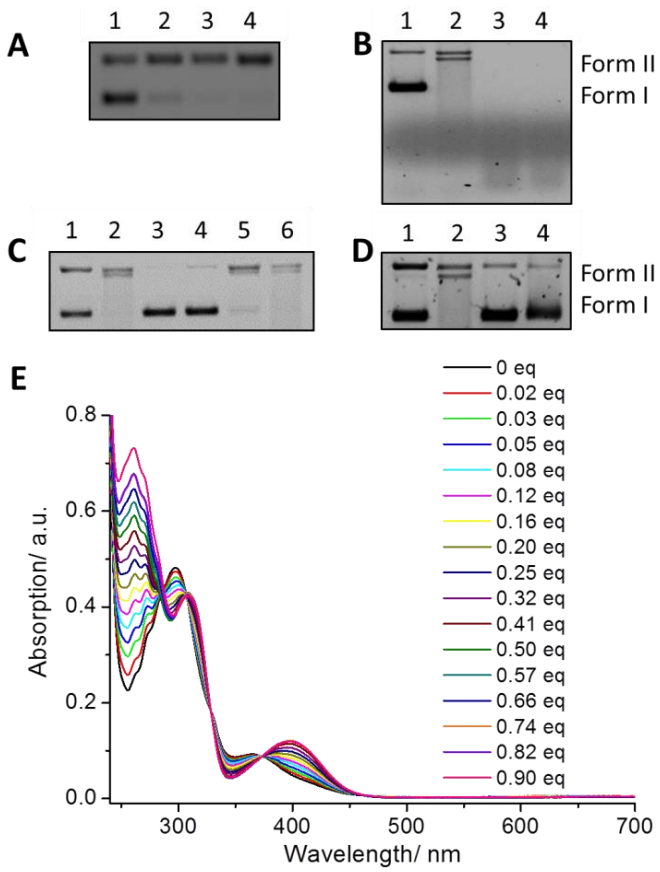

Figure 1. (A) Concentration-dependent DNA cleavage by **4** after 24 h incubation, Lane 1: DNA only, Lane 2-4: DNA + 10, 25, and 50 µM of **4**. (B) Effect of ascorbic acid on **4**-mediated DNA cleavage after 24 h incubation, Lane 1: DNA only, Lane 2-4: DNA + 10, 25, and 50 µM of **4** with 10 equivalents of ascorbic acid. (C) Inhibition of **4**-mediated DNA cleavage by ROS scavengers after 24 h incubation. a) Lane 1: DNA only, Lane 2: DNA + **4** (10 µM), Lane 3-6: DNA + **4** (10 µM) + NaN_3 (40 mM), KI (40 mM), DMSO (10 mM), or ^{t}BuOH (10 mM). (D) Inhibition of **4**-mediated DNA cleavage by DNA minor and major groove binders after 24 h incubation, Lane 1: DNA only, Lane 2: DNA + **4** (10 µM), Lane 3: DNA + **4** (10 µM) + methyl green (50 µM), Lane 4: DNA + **4** (10 µM) + DAPI (50 µM). (E) Representative UV-Vis trace of **4** (50 µM) upon addition of ct-DNA (0 - 0.9 equivalence).

Lipophilicity and Stability in Biologically Relevant Solutions

The lipophilicity of **1**-**4** was determined by measuring the extent to which it partitioned between octanol and water, P. The experimentally determined Log P values varied from -0.200 ± 0.011 to -0.093 ± 0.015 (Table S1). The position of the methoxy group appears to subtly affect lipophilicity, with hydrophobicity increasing in the following order; **4** > **3** > **1** > **2**. The amphiphilic nature of **1**-**4** suggests that the copper(II) complexes should be readily taken up by cells and soluble in aqueous solutions. UV-Vis spectroscopy studies were carried out to assess the stability of **4**, taken as a representative member of the copper(II) complexes, in biological relevant solutions. In PBS, **4** (50 µM) is reasonably stable over the course of 24 h at 37 ^{o}C (Figure S12). In the presence of ascorbic acid or glutathione (10 equivalents in PBS), the absorption of **4** (50 µM) changed dramatically over the course of 24 h at 37 ^{o}C, yielding spectra reminiscent of free naproxen (Figure S13-15). Upon incubation of concentrated PBS:DMSO (95:5) solutions of **4** (250 µM) with ascorbic acid or glutathione (10 equivalence in PBS) for 24h at 37 ^{o}C, the d-d transition band (637 nm) associated to the copper(II) center decreased markedly suggesting reduction to copper(I) (Figure S16-17). This was further evidenced by adding bathocuproine disulfonate (BCS, 2 equivalence), a strong copper(I) chelator, which produced a characteristic absorption band at 480 nm corresponding to $[Cu^{I}(BCS)_2]^{3-}$ (Figure S18-19).[19] Taken together, the UV-Vis stability studies suggest that **4** is reduced from the Cu(II) to Cu(I) form under reducing conditions and that this facilitates the release of naproxen.

Bulk Cancer and Cancer Stem Cell Potency

To determine the CSC and non-CSC potency of **1**-**4**, two human mammary epithelial cell lines (HMLER and HMLER-shEcad cells) were used. HMLER cells contain a stable CSC-like population of 5-8% and HMLER-shEcad cells express a *ca.* 90% CSC-like population.[20] The cytotoxicity of **1**-**4** towards HMLER and HMLER-shEcad cells was measured using the MTT [3-(4,5-di-methylthiazol-2-yl)-2,5-diphenyltetrazolium bromide] assay after 72 h incubation. IC_{50} values (concentrations required to induce 50% cell death) were determined from dose–response curves (Figure S20-23) and are summarized in Table 1. Three of the complexes (**1**, **3**, and **4**) displayed micromolar potency towards CSC-enriched HMLER-shEcad cells and CSC-depleted HMLER cells. Notably, **4** is the most potent complex within the series. Unlike salinomycin, a "gold standard" CSC-selective agent[20] and the CSC-selective copper(II)-phenanthroline-NSAID complexes recently reported by our group,[8b,8e] **4** indiscriminately kills CSCs and bulk cancer cells. Therefore, **4** has the potential to remove cancer cell populations in their entirety (bulk cancer cells and CSCs) with a single dose. The trend between the position of the methoxy group and lipophilicity (noted previously) is loosely observed for potency against bulk cancer (HMLER) and CSCs (HMLER-shEcad). The **L**^{2}-bearing complex, **2** was the most hydrophilic within the series and the least cytotoxic towards bulk cancer cells and CSCs (>100 µM). As a measure of therapeutic potential, we conducted cytotoxicity studies with normal human fibroblast GM05757 cells (Figure S24 and Table S2). In general, **1**-**4** displayed similar potency for GM05757 cells as bulk cancer and CSCs. Only complex **4** displayed lower potency (2-fold) for the normal fibroblast cell line than for the cancer cell lines.

Table 1. IC_{50} values of the copper(II) complexes, **1-4** and salinomycin against HMLER and HMLER-shEcad cells.

Compound	HMLER IC_{50} [μM][a]	HMLER-shEcad IC_{50} [μM][a]
1	61.0 ± 0.9	56.8 ± 3.1
2	> 100	> 100
3	61.5 ± 2.2	67.4 ± 4.7
4	37.6 ± 3.3	36.0 ± 4.6
salinomycin[b]	11.4 ± 0.42	4.2 ± 0.4

[a] Determined after 72 h incubation (mean of three independent experiments ± SD). [b] Taken from reference 8b.

Inhibition of Mammosphere Formation

Breast CSCs cultured in anchorage-independent, serum-free conditions, over extended periods of time, form three-dimensional, tumor-like structures called mammospheres.[21] The capacity of a given agent to inhibit mammosphere formation from single cell suspensions provides a reliable marker for CSC potency. The ability of **1**-**4** to inhibit mammosphere formation was assessed using an inverted microscope. Treatment with **1**-**3** (at the IC_{20} value after 5 days of incubation) did not significantly affect the number or size of mammospheres formed (p = 0.08 for **1**, p = 0.35 for **2**, and p = 0.31 for **3**) (Figure 2). The addition of **4** (at the IC_{20} value after 5 days of incubation) significantly reduced the number of mammospheres formed (38%, $p < 0.05$). The size of mammospheres formed was also markedly reduced upon incubation with **4** (Figure 2). The number and size of mammospheres formed decreased to a slightly better extent upon treatment with salinonmycin (at the IC_{20} value after 5 days of incubation) (Figure 2).

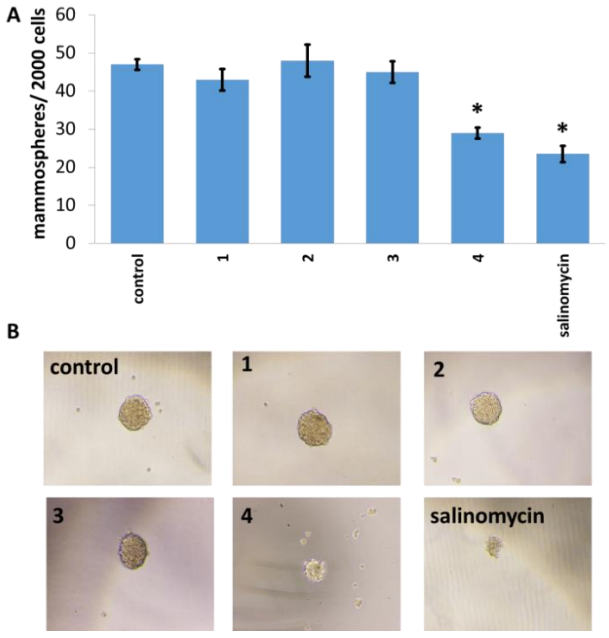

Figure 2. (A) Quantification of mammosphere formation with HMLER-shEcad cells untreated and treated with **1**-**4** and salinomycin at their respective IC_{20} values for 5 days. Error bars = SD and Student *t-test*, * = $p < 0.05$. (B) Representative bright-field images (× 10) of the mammospheres in the absence and presence of **1**-**4** and salinomycin at their respective IC_{20} values.

Cellular Mechanism of Action

Cell uptake studies were performed to determine the CSC permeability of **1**-**4**. Specifically, HMLER-shEcad cells were incubated with **1**-**4** at a non-lethal dose (10 μM for 24 h) and the copper content was determined by inductively coupled plasma mass spectrometry (ICP-MS). As shown in Figure S25, all the complexes were taken up readily by HMLER-shEacd cells, with whole cell uptake ranging from 81.2 ± 1.7 ppb of Cu/ million cells for **3** to 336.8 ± 8.0 ppb of Cu/ million cells for **1**. No correlation was noted between whole cell uptake and cytotoxicity of **1**-**4**. For the most effective complex, **4**, fractionation studies were carried to determine cell localization (Figure 3A). A substantial amount of internalized **4** (25%) was found in the nucleus, providing assess to genomic DNA. This may be attributed to the naproxen moiety, which is known to target COX-2 localized on the nuclear envelop.[22] An appreciated amount of internalized **4** was also observed in the cytoplasm (57%). Taken together, the fractionation studies suggest that **4**-induced cell toxicity could be related to genomic DNA-dependent or -independent mechanisms.

Copper(II) complexes bearing Schiff base ligands are known to induce cell death by elevating intracellular ROS levels.[12] To investigate if **4**-indued toxicity is related to ROS production, intracellular ROS levels were quantified at different exposure times using 6-carboxy-2',7'-dichlorodihydrofluorescein diacetate (DCFH-DA), a well-established ROS indicator. Upon incubation of HMLER-shEcad cells with **4** (50 μM) for 6 h a marked increase (27%) in intracellular ROS levels was observed compared to the untreated control cells (Figure S26). Exposure of **4** (50 μM) for longer periods (12 and 24 h) did not result in ROS increase relative to untreated cells, suggesting that **4**-mediated ROS generation is time-dependent (Figure S26). Similar time-dependent ROS production properties have been reported for other metal complexes.[23] H_2O_2-treated (150 μM for 6, 12, and 24 h) HMLER-shEcad cells exhibited a significant increase ($p < 0.01$) in ROS levels (Figure S27). Both **4**- (after 6 h exposure) and H_2O_2- (after 6, 12, and 24 h exposure) induced ROS production was attenuated in the presence of *N*-acetylcysteine (2.5 mM), a ROS scavenger (Figure S26-27). Overall, this suggests that **4**-induced cell death could be associated to intracellular ROS generation.

As **4** was found to increase intracellular ROS levels, enter the nucleus, and displays redox-mediated nuclease activity in cell-free systems, immunoblotting studies were carried out to determine if **4** induces DNA damage in CSCs. HMLER-shEcad cells dosed with **4** (5-20 μM for 72 h) exhibited a marked increase in the expression of phosphorylated H2AX (γH2AX) and a slight increase in the expression of phosphorylated CHK2, implicative of DNA damage (Figure S28).[24] DNA damage, when left unrepaired, can lead to apoptosis,[25] therefore the expression of proteins associated to apoptosis were monitored. HMLER-shEcad cells treated with **4** (5-20 μM for 72 h) exhibited a clear increase in the level of cleaved caspase 3 and 7 compared to untreated control cells, indicative of caspase-dependent apoptosis (Figure S28). Collectively, the immunoblotting studies show that **4** induces DNA damage and apoptotic CSC death.

Elevated levels of COX-2 have been linked to poor prognostic markers in cancer patients such as high tumor grade

and large tumor size.[26] Further, COX-2 is implicated in CSC regulation and thought to promote CSC-like properties such as stemness, tumorosphere formation, and metastatic propensity.[27] As complex **4** contains a naproxen moiety, an established COX-2 inhibitor, flow cytometric studies were conducted to determine if the mechanism of action of **4** involved COX-2 inhibition. HMLER-shEcad cells pre-treated with lipopolysaccharide (LPS) (5 μM for 24 h), to increase basal COX-2 levels, and dosed with **4** (12.5-50 μM for 48 h) displayed a noticeable decrease in COX-2 expression compared to untreated cells (Figure 3B). A similar decrease in COX-2 expression was also noted for naproxen-treated (20 μM for 48 h) HMLER-shEcad cells (Figure S29). This suggests that the cytotoxic effect of **4** may involve COX-2 downregulation. To determine if **4** induces COX-2 dependent CSC death, cytotoxicity studies were performed with HMLER-shEcad in the presence and absence of prostaglandin E2 (PGE2) (20 μM, 72 h), the functional product of COX-2-mediated arachidonic acid metabolism. The potency of **4** towards HMLER-shEcad cells decreased significantly in the presence of PGE2 (Figure 3C), suggesting that **4** induces COX-2-dependent CSC death.

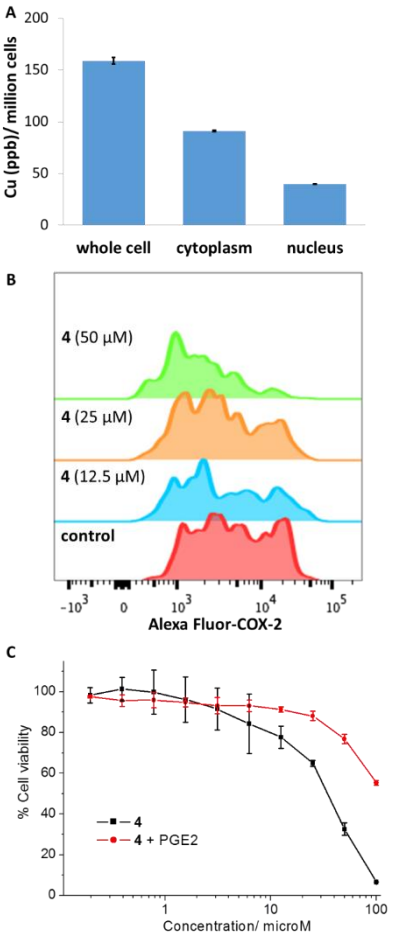

Figure 3. (A) Copper content in whole cell, cytoplasm, and nucleus fractions isolated from HMLER-shEcad cells treated with **4** (10 μM for 24 h). (B) Representative histograms displaying the green fluorescence emitted by anti-COX-2 Alexa Fluor 488 nm antibody-stained HMLER-shEcad cells treated with LPS (2.5 μM) for 24 h (red) followed by 48 h in media containing **4** (12.5 - 50 μM, blue, orange, and green). (C) Representative dose-response curves for the treatment of HMLER-shEcad cells with **4** after 72 incubation in the presence and absence of PGE2 (20 μM).

Conclusion

In summary, we report four new copper(II) complexes with vanillin Schiff base derivatives and naproxen. DNA cleavage and binding studies suggest that the most effective complex, **4** binds to DNA via the grooves ($1.3 \pm 0.3 \times 10^5$ M^{-1}) and induces oxidative cleavage (at 10 μM). Hydrogen peroxide (H_2O_2) and singlet oxygen ($^1O_2$) were identified to be the main ROS intermediates formed during the DNA cleavage process. Complex **4** was found to kill bulk breast cancer cells and breast CSCs with micromolar toxicity (37.6 ± 3.3 and 36.0 ± 4.6 μM respectively), and potently inhibit mammosphere formation (38% decrease upon treatment at IC_{20} value for 5 days) to a similar extent as salinomycin. Given that several copper(II) complexes reported in literature are known to cleave DNA and exhibit toxicity in the micromolar range, the true anticancer potential of these compounds need to be determined using in vivo cancer models. We are in the process of initiating in vivo studies in mice with **4**. Mechanistic studies suggest that **4** increases intracellular ROS levels at short exposure times (6 h), damages DNA, downregulates COX-2 expression, and triggers caspase-dependent apoptosis. As **4** displays equal potency towards bulk cancer cells and CSCs, it could potentially remove entire cancer populations with a single dose. This study not only shows that copper(II) complexes with vanillin Schiff base derivatives and NSAIDs warrant further investigation as anticancer agents capable of eliminating heterogenous tumor populations, but it also provides insight into copper-induced cell death.

Experimental Section

Materials and Methods

All synthetic procedures were performed under normal atmospheric conditions. Fourier transform infrared (FTIR) spectra were recorded with a IRAffinity-1S Shimadzu spectrophotometer. High resolution electron spray ionisation mass spectra were recorded on a BrukerDaltronics Esquire 3000 spectrometer by Dr. Lisa Haigh (Imperial College London). UV-Vis absorption spectra were recorded on a Cary100 UV-Vis spectrophotometer. Elemental analysis of the compounds prepared was performed commercially by London Metropolitan University. 2-(Methylthio)ethan-1-amine, 2-hydroxy-3-methoxybenzaldehyde, 2-hydroxy-4-methoxybenzaldehyde, 2-hydroxy-5-methoxybenzoic acid, and 2-hydroxy-6-methoxybenzaldehyde were purchased from Sigma Aldrich and used as received. For the high concentration UV studies (250 μM), a 10 mM stock solution of **4** in DMSO was initially prepared. The copper concentration of the stock solution was determined by inductively coupled plasma mass spectrometry (ICP-MS, PerkinElmer NexION 350D). The stock solution was diluted in PBS to the working concentration.

Synthesis

(E)-2-methoxy-6-(((2-(methylthio)ethyl)imino)methyl)phenol (L[1]): A mixture of 2-(methylthio)ethan-1-amine (91 mg, 1 mmol) and 2-hydroxy-3-methoxybenzaldehyde (152 mg, 1 mmol) were refluxed in ethanol (20 mL) for 16 h. The reaction mixture was then evaporated under vacuum to afford a yellow oil. Yield: 207 mg (92%). ^{1}H NMR (400 MHz, $CDCl_3$): δ 13.69 (s, 1H), 8.37 (s, 1H), 6.94-6.89 (m, 2H), 6.82 (t, 1H), 3.91(s, 3H), 3.82 (t, 2H), 2.83 (t, 2H), 2.14 (s, 3H). ^{13}C NMR (100 MHz, $CDCl_3$): δ 165.9, 151.7, 148.5, 123.0, 118.5, 118.0, 114.1, 58.9, 56.1, 35.1, 16.1. IR (solid, cm^{-1}): 1631, 1462, 1249, 1080, 1049, 965, 839, 779, 733. API-MS (positive) *m*/*z*: 226.2 $[M+H]^+$; (negative) *m*/*z*: 224.2 $[M-H]^-$.

(E)-5-methoxy-2-(((2-(methylthio)ethyl)imino)methyl)phenol (L^2): A mixture of 2-(methylthio)ethan-1-amine (91 mg, 1 mmol) and 2-hydroxy-4-methoxybenzaldehyde (152 mg, 1 mmol) were refluxed in ethanol (20 mL) for 16 h. The reaction mixture was then evaporated under vacuum to afford a yellow solid. Yield: 202 mg (90%). ^{1}H NMR (400 MHz, $CDCl_3$): δ 13.75 (s, 1H), 8.23 (s, 1H), 7.13 (d, 1H), 6.44-6.39 (m, 2H), 3.81(s, 3H), 3.75 (t, 2H), 2.81 (t, 2H), 2.14 (s, 3H). ^{13}C NMR (100 MHz, $CDCl_3$): δ 165.1, 164.7, 163.6, 132.7, 112.3, 106.5, 101.2, 57.9, 55.9, 36.2, 16.0. IR (solid, cm^{-1}): 1641, 1611, 1513, 1481, 1440, 1362, 1328, 1269, 1217, 1170, 1111, 1011, 969, 895, 842, 788, 760, 668, 569, 512. API-MS (positive) *m*/*z*: 226.2 $[M+H]^+$, 258.1 $[M+CH_3OH+H]^+$.

(E)-4-methoxy-2-(((2-(methylthio)ethyl)imino)methyl)phenol (L^3): A mixture of 2-(methylthio)ethan-1-amine (91 mg, 1 mmol) and 2-hydroxy-5-methoxybenzoic acid (152 mg, 1 mmol) were refluxed in ethanol (20 mL) for 16 h. The reaction mixture was then evaporated under vacuum to afford a yellow oil. Yield: 211 mg (94%). ^{1}H NMR (400 MHz, $CDCl_3$): δ 12.75 (s, 1H), 8.34 (s, 1H), 6.95-6.89 (m, 2H), 6.79 (d, 1H), 3.81 (t, 2H), 3.78 (s, 3H), 2.83 (t, 2H), 2.14 (s, 3H). ^{13}C NMR (100 MHz, $CDCl_3$): δ 165.6, 155.2, 152.0, 119.4, 118.3, 117.8, 114.9, 59.2, 55.9, 36.1, 16.0. IR (solid, cm^{-1}): 1636, 1490, 1267, 1224, 1156, 1034, 813, 786. API-MS (positive) *m*/*z*: 226.2 $[M+H]^+$; (negative) *m*/*z*: 259.8 $[M+Cl]^-$.

(E)-3-methoxy-2-(((2-(methylthio)ethyl)imino)methyl)phenol (L^4): A mixture of 2-(methylthio)ethan-1-amine (91 mg, 1 mmol) and 2-hydroxy-6-methoxybenzaldehyde (152 mg, 1 mmol) were refluxed in ethanol (20 mL) for 16 h. The reaction mixture was then evaporated under vacuum to afford a yellow oil. Yield: 214 mg (95%). ^{1}H NMR (400 MHz, $CDCl_3$): δ 14.29 (s, 1H), 8.83 (s, 1H), 7.22 (t, 1H), 6.54 (d, 1H), 6.30 (d, 1H), 3.84 (s, 3H), 3.79 (t, 2H), 2.81 (t, 2H), 2.15 (s, 3H). IR (solid, cm^{-1}): 1622, 1463, 1374, 1246, 1092, 1052, 783, 726. API-MS (positive) *m*/*z*: 226.2 $[M+H]^+$.

Cu(L^1)(naproxen) (1): Naproxen (69.08 mg, 0.3 mmol) dissolved in ethanol (10 mL) was added dropwise under stirring to a mixture of **L^1** (67.5 mg, 0.3 mmol) and $Cu(NO_3)_2{\cdot}3H_2O$ (72 mg, 0.3 mmol) in ethanol (10 mL). Triethylamine was added to the mixture to adjust the pH to 7. The mixture was refluxed at 80 ^{o}C for 24 h. The resulting precipitate was filtered off, and the filtrate was evaporated to dryness. The resulting solid was washed thoroughly with water and diethyl ether. The product was isolated as a green solid (74 mg, 48%). IR (solid, cm^{-1}): 1627, 1603, 1563, 1469, 1453, 1390, 1301, 1247, 1227, 1214, 1171, 1071, 1029, 927, 855, 780, 739. HR ESI-MS Calcd. for $C_{25}H_{30}CuNO_5S$ [reduced form, M+H]$^+$: 519.1141 a.m.u. Found [reduced form, M+H]$^+$: 519.0647 a.m.u. Anal. Calcd. for **1**·$2H_2O$, $C_{25}H_{31}CuNO_7S$: C, 54.29; H, 5.65; N, 2.53. Found: C, 53.90; H, 5.13; N, 2.92.

Cu(L^2)(naproxen) (2): Naproxen (69.08 mg, 0.3 mmol) dissolved in ethanol (10 mL) was added dropwise under stirring to a mixture of **L^2** (67.5 mg, 0.3 mmol) and $Cu(NO_3)_2{\cdot}3H_2O$ (72 mg, 0.3 mmol) in ethanol (10 mL). Triethylamine was added to the mixture to adjust the pH to 7. The mixture was refluxed at 80 ^{o}C for 24 h. The resulting precipitate was filtered off, and the filtrate was evaporated to dryness. The resulting solid was washed thoroughly with water and diethyl ether. The product was isolated as a green solid (43 mg, 28%). IR (solid, cm^{-1}): 1606, 1583, 1506, 1483, 1454, 1397, 1367, 1271, 1232, 1212, 1163, 1033, 928, 899, 855, 817, 749, 704. HR ESI-MS Calcd. for $C_{25}H_{30}CuNO_5S$ [reduced form, M+H]$^+$: 519.1141 a.m.u. Found [reduced form, M+H]$^+$: 519.0680 a.m.u. Anal. Calcd. for compound **2,** $C_{25}H_{27}CuNO_5S$: C, 58.07; H, 5.26; N, 2.71. Found: C, 58.03; H, 5.17; N, 2.83.

Cu(L^3)(naproxen) (3): Naproxen (69.08 mg, 0.3 mmol) dissolved in ethanol (10 mL) was added dropwise under stirring to a mixture of **L^3** (67.5 mg, 0.3 mmol) and $Cu(NO_3)_2{\cdot}3H_2O$ (72 mg, 0.3 mmol) in ethanol (10 mL). Triethylamine was added to the mixture to adjust the pH to 7. The mixture was refluxed at 80 ^{o}C for 24 h. The resulting precipitate was filtered off, and the filtrate was evaporated to dryness. The resulting solid was washed thoroughly with water and diethyl ether. The product was isolated as a green solid (31 mg, 20%). IR (solid, cm^{-1}): 1633, 1604, 1585, 1506, 1483, 1457, 1406, 1393, 1366, 1268, 1229, 1213, 1161, 1032, 928, 853, 809, 749. HR ESI-MS Calcd. for $C_{25}H_{30}CuNO_5S$ [reduced form, M+H]$^+$: 519.1141 a.m.u. Found [reduced form, M+H]$^+$: 519.0668 a.m.u. Anal. Calcd. for compound **3,** $C_{25}H_{27}CuNO_5S$: C, 58.07; H, 5.26; N, 2.71. Found: C, 58.25; H, 5.14; N, 2.60.

Cu(L^4)(naproxen) (4): Naproxen (69.08 mg, 0.3 mmol) dissolved in ethanol (10 mL) was added dropwise under stirring to a mixture of **L^4** (67.5 mg, 0.3 mmol) and $Cu(NO_3)_2{\cdot}3H_2O$ (72 mg, 0.3 mmol) in ethanol (10 mL). Triethylamine was added to the mixture to adjust the pH to 7. The mixture was refluxed at 80 ^{o}C for 24 h. The resulting precipitate was filtered off, and the filtrate was evaporated to dryness. The resulting solid was washed thoroughly with water and diethyl ether. The product was isolated as a green solid (104 mg, 67%). IR (solid, cm^{-1}): 1607, 1585, 1548, 1396, 1363, 1252, 1212, 1105, 1034, 927, 856, 818, 788, 750, 729, 616, 548. HR ESI-MS Calcd. for $C_{25}H_{30}CuNO_5S$ [reduced form, M+H]$^+$: 519.1141 a.m.u. Found [reduced form, M+H]$^+$: 519.0692 a.m.u. Anal. Calcd. for compound **4,** $C_{25}H_{27}CuNO_5S$: C, 58.07; H, 5.26; N, 2.71. Found: C, 57.95; H, 5.31; N, 2.80.

DNA Cleavage Studies. Plasmid DNA (pUC19) was purchased from Invitrogen. The DNA cleavage activity of **1**-**4** was determined by monitoring the conversion of supercoiled plasmid DNA (form I) to nicked circular DNA (form II) in Tris-HCl buffer (5 mM, pH 7.4), using agarose-gel electrophoresis. To probe the effect of compound concentration on cleavage, solutions containing DNA (100 ng) and **1**-**4** (0-50 μM), with a total reaction volume of 20 μL, were incubated at 37 ^{o}C for 24 h. To determine the oxidative cleavage mechanism, solutions containing DNA (100 ng), **4** (10 μM), and various radical scavenges (10 mM or 40 mM of KI, DMSO, ^{t}BuOH, and NaN_3), with a total reaction volume of 20 μL, were incubated at 37 ^{o}C for 24 h. Reactions were also conducted in the presence of 10 equivalents of ascorbic acid, and in the presence of methyl green (50 μM) and DAPI (50 μM). After incubation, loading buffer (5 μL, containing 0.25% bromophenol blue, 0.25% xylene cyanol, and 60% glycerol) was added and reaction mixtures were immediately loaded onto a 1% agarose gel containing ethidium bromide (1.0 mg mL^{-1}). The DNA fragments were separated by applying 60 V for 2 h in Tris-acetate EDTA (TAE) buffer. The DNA bands were analyzed under UV light using a Fujifilm Image Reader LAS-3000.

UV-Vis Tritation Studies.
To determine the binding constants of **4** with ct-DNA, **4** (50 μM) was titrated with concentrated solutions of ct-DNA (mM) in Tris-HCl buffer (5 mM, pH 7.4). The binding constants were obtained by fitting the data to a reciprocal plot of $D/\Delta\varepsilon_{ap}$ versus D using the following equation: $D/\Delta\varepsilon_{ap} = D/\Delta\varepsilon - 1/(\Delta\varepsilon \times K)$ where the concentration of DNA is expressed in terms of base pairs (determined by measuring the absorption at 260 nm and the appropriate extinction coefficients), the apparent molar extinction coefficient $\varepsilon_a = A_{observed}/[Complex]$, $\Delta\varepsilon_{ap} = [\varepsilon_a - \varepsilon_f]$ and $\Delta\varepsilon = [\varepsilon_b - \varepsilon f]$. ε_b is the extinction coefficient of the DNA bound complex, and ε_f is the extinction coefficient of the free complex. The UV-Vis spectra were recorded on an Agilent Cary100 UV-Vis spectrophotometer. A 1 cm path- length quartz cuvette was used to carry out the measurements.

Ethidium Bromide and DAPI Displacement Studies.
To a mixture of ethidium bromide (1 μM) or DAPI (1 μM) and ct-DNA (20 μM) in Tris-HCl buffer (5 mM, pH 7.4), an increasing amount **4**, **L^4**, or naproxen (0-200 μM) was added. The emission spectrum was recorded between 550 and 800 nm with an excitation wavelength of 526 nm. The fluorescence studies were performed on a Varian Cary Eclipse spectrometer.

Measurement of Water-Octanol Partition Coefficient (Log P). The log P value for **1**-**4** was determined using the shake-flask method and UV-Vis spectroscopy. The octanol used in this experiment was pre-saturated with water. An aqueous solution of **1**-**4** (500 μL, 100 μM) was incubated with octanol (500 μL) in a 1.5 mL tube. The tube was shook at room temperature for 48 h. The two phases were separated by centrifugation and **1**-**4** content in each phase was determined by UV-Vis spectroscopy.

Cell Lines and Cell Culture Conditions. The human mammary epithelial cell lines, HMLER and HMLER-shEcad were kindly donated by Prof. R. A. Weinberg (Whitehead Institute, MIT). HMLER and HMLER-shEcad cells were maintained in Mammary Epithelial Cell Growth Medium (MEGM) with supplements and growth factors (BPE, hydrocortisone, hEGF, insulin, and gentamicin/amphotericin-B). The GM05757 normal fibroblast cell line was acquired from the American Type Culture Collection (ATCC, Manassas, VA, USA) and maintained in Dulbecco's Modified Eagle's Medium (DMEM) supplemented with 10% fetal bovine serum and 1% penicillin/streptomycin. The cells were grown at 310 K in a humidified atmosphere containing 5% CO_2.

Cytotoxicity MTT assay. The colourimetric MTT assay was used to determine the toxicity of **1**-**4**. HMLER, HMLER-shEcad, or GM05757 (5 ×

10^3) were seeded in each well of a 96-well plate. After incubating the cells overnight, various concentrations of the compounds (0.2-100 μM), were added and incubated for 72 h (total volume 200 μL). Stock solutions of the compounds were prepared as 10 mM solutions in DMSO and diluted using media. The final concentration of DMSO in each well was 0.5% and this amount was present in the untreated control as well. After 72 h, 20 μL of a 4 mg/mL solution of MTT in PBS was added to each well, and the plate was incubated for an additional 4 h. The MEGM/MTT or DMEM/MTT mixture was aspirated and 200 μL of DMSO was added to dissolve the resulting purple formazan crystals. The absorbance of the solutions in each well was read at 550 nm. Absorbance values were normalized to (DMSO-containing) control wells and plotted as concentration of test compound versus % cell viability. IC_{50} and IC_{20} values were interpolated from the resulting dose dependent curves. The IC_{50} and IC_{20} values correspond to the concentration required to decrease cell viability by 50 % or 20% and were calculated from dose–response curves. The reported IC_{50} values are the average of three independent experiments, each consisting of six replicates per concentration level (overall n = 18).

Tumorsphere Formation. HMLER-shEcad cells (5×10^3) were plated in ultralow-attachment 96-well plates (Corning) and incubated in MEGM supplemented with B27 (Invitrogen), 20 ng/mL EGF, and 4 μg/mL heparin (Sigma) for 5 days. Studies were conducted in the absence and presence of **1**-**4** and salinomycin. Mammospheres treated with **1**-**4** and salinomycin (at their respective IC_{20} values, 5 days) were counted and imaged using an inverted microscope.

Cellular Uptake. To measure the cellular uptake of **1**-**4** *ca.* 1 million HMLER-shEcad cells were treated with **1**-**4** (10 μM) at 37 ºC for 24 h. After incubation, the media was removed, the cells were washed with PBS (2 mL × 3), harvested, and centrifuged. The cellular pellets were dissolved in 65% HNO_3 (250 μL) overnight. For **4**, cellular pellets were also used to determine the copper content in the nuclear and cytoplasmic fractions. The Thermo Scientific NE-PER Nuclear and Cytoplasmic Extraction Kit were used to extract and separate the nuclear and cytoplasmic, fractions. The fractions were dissolved in 65% HNO_3 overnight (250 μL final volume). All samples were diluted 5-fold with water and analysed using inductively coupled plasma mass spectrometry (ICP-MS, PerkinElmer NexION 350D). Copper levels are expressed as Cu (ppb) per million cells. Results are presented as the mean of five determinations for each data point.

Intracellular ROS Assay. HMLER-shEcad cells (5×10^3) were seeded in each well of a 96-well plate. After incubating the cells overnight, they were treated with **4** or H_2O_2 (50 and 150 μM for 6, 12, and 24 h), in the presence or absence of *N*-acetylcysteine (2.5 mM), and incubated with 6-carboxy-2′,7′-dichlorodihydrofluorescein diacetate (20 μM) for 30 min. The intracellular ROS level was determined by measuring the fluorescence of the solutions in each well at 529 nm (λ_{ex} = 504 nm).

Immunoblotting Analysis. HMLER-shEcad cells (5×10^5 cells) were incubated with **4** (5-20 μM for 72 h) at 37 ºC. Cells were washed with PBS, scraped into SDS-PAGE loading buffer (64 mM Tris-HCl (pH 6.8)/ 9.6% glycerol/ 2% SDS/ 5% β-mercaptoethanol/ 0.01% Bromophenol Blue), and incubated at 95 ºC for 10 min. Whole cell lysates were resolved by 4-20 % sodium dodecylsulphate polyacylamide gel electrophoresis (SDS-PAGE; 200 V for 25 min) followed by electro transfer to polyvinylidene difluoride membrane, PVDF (350 mA for 1 h). Membranes were blocked in 5% (w/v) non-fat milk in PBST (PBS/0.1% Tween 20) and incubated with the appropriate primary antibodies (Cell Signalling Technology). After incubation with horseradish peroxidase-conjugated secondary antibodies (Cell Signalling Technology), immune complexes were detected with the ECL detection reagent (BioRad) and analysed using a chemiluminescence imager (Amersham Imager 600).

Flow cytometry. HMLER-shEcad cells were seeded in 6-well plates (at a density of 5×10^5 cells/ mL) and the cells were allowed to attach overnight. The cells were treated with lipopolysaccharide (LPS) (2.5 μM for 24 h), and then treated with **4** (12.5-50 μM) or naproxen (20 μM) and incubated for a further 48 h. The cells were then harvested by trypsinization, fixed with 4% paraformaldehyde (at 37 ºC for 10 min), permeabilized with ice-cold methanol (for 30 min), and suspended in PBS (200 μL). The Alexa Fluor® 488 nm labelled anti-COX-2 antibody (5 μL) was then added to the cell suspension and incubated in the dark for 1 hr. The cells were then washed with PBS (1 mL) and analysed using a FACSCanto II flow cytometer (BD Biosciences) (10,000 events per sample were acquired). The FL1 channel was used to assess COX-2 expression. Cell populations were analysed using the FlowJo software (Tree Star).

Acknowledgements ((optional))

K.S. is supported by an Early Career Fellowship (ECF-2014-178) from the Leverhulme Trust. A.E. received financial support from a King's College London Faculty Graduate School International Studentship. C.L. thanks the Natural Science Foundation of China (Grant No.21401078) for financial support. We are grateful to Prof. Robert Weinberg for providing the HMLER and HMLER-shEcad cell lines used in this study.

Keywords: copper • bioinorganic chemistry • cancer •antitumor agents • nonsteroidal anti-inflammatory drugs

[1] M. C. Cabrera, R. E. Hollingsworth, E. M. Hurt, *World J. Stem Cells* **2015**, *7*, 27-36.
[2] J. N. Rich, *Medicine* **2016**, *95*, S2-7.
[3] M. Z. Ratajczak, *Folia Histochem. Cytobiol.* **2005**, *43*, 175-181.
[4] a) J. Marx, *Science* **2007**, *317*, 1029-1031; bD. R. Pattabiraman, R. A. Weinberg, *Nat. Rev. Drug Discov.* **2014**, *13*, 497-512.
[5] a) L. N. Abdullah, E. K. Chow, *Clin. Transl. Med.* **2013**, *2*, 3; b) J. Kaiser, *Science* **2015**, *347*, 226-229; c) K. Rycaj, D. G. Tang, *Int. J. Radiat. Biol.* **2014**, *90*, 615-621.
[6] a) K. Chen, Y.-h. Huang, J.-l. Chen, *Acta. Pharmacol. Sin.* **2013**, *34*, 732-740; b) W. Chen, J. Dong, J. Haiech, M. C. Kilhoffer, M. Zeniou, *Stem Cells Int.* **2016**, *2016*, 1740936; c) Y. X. Feng, E. S. Sokol, C. A. Del Vecchio, S. Sanduja, J. H. Claessen, T. A. Proia, D. X. Jin, F. Reinhardt, H. L. Ploegh, Q. Wang, P. B. Gupta, *Cancer Discov.* **2014**, *4*, 702-715; d) R. Lamb, H. Harrison, J. Hulit, D. L. Smith, M. P. Lisanti, F. Sotgia, *Oncotarget* **2014**, *5*, 11029-11037; e) Q. E. Wang, *World J. Biol. Chem.* **2015**, *6*, 57-64.
[7] X. Ning, J. Shu, Y. Du, Q. Ben, Z. Li, *Cancer Biol. Ther.* **2013**, *14*, 295-303.
[8] a) N. Aztopal, D. Karakas, B. Cevatemre, F. Ari, C. Icsel, M. G. Daidone, E. Ulukaya, *Bioorg. Med. Chem.* **2017**, *25*, 269-276; b) J. N. Boodram, I. J. McGregor, P. M. Bruno, P. B. Cressey, M. T. Hemann, K. Suntharalingam, *Angew. Chem. Int. Ed.* **2016**, *55*, 2845-2850; c) P. Cressey, A. Eskandari, P. Bruno, C. Lu, M. Hemann, K. Suntharalingam, *ChemBioChem* **2016**; d) P. Cressey, A. Eskandari, K. Sunthharalingam, *Inorganics* **2017**, *5*, 12; e) A. Eskandari, J. N. Boodram, P. B. Cressey, C. Lu, P. M. Bruno, M. T. Hemann, K. Suntharalingam, *Dalton Trans.* **2016**, *45*, 17867-17873; f) M. Gonzalez-Bartulos, C. Aceves-Luquero, J. Qualai, O. Cusso, M. A. Martinez, S. Fernandez de Mattos, J. A. Menendez, P. Villalonga, M. Costas, X. Ribas, A. Massaguer, *PloS one* **2015**, *10*, e0137800; g) C. T. Lum, A. S. Wong, M. C. Lin, C. M. Che, R. W. Sun, *Chem. Commun.* **2013**, *49*, 4364-4366; h) K. Suntharalingam, W. Lin, T. C. Johnstone, P. M. Bruno, Y. R. Zheng, M. T. Hemann, S. J. Lippard, *J. Am. Chem. Soc.* **2014**, *136*, 14413-14416.
[9] a) M. Diehn, R. W. Cho, N. A. Lobo, T. Kalisky, M. J. Dorie, A. N. Kulp, D. Qian, J. S. Lam, L. E. Ailles, M. Wong, B. Joshua, M. J. Kaplan, I. Wapnir, F. M. Dirbas, G. Somlo, C. Garberoglio, B. Paz, J. Shen, S. K. Lau, S. R. Quake, J. M. Brown, I. L. Weissman, M. F. Clarke, *Nature* **2009**, *458*, 780-783; b) X. Shi, Y. Zhang, J. Zheng, J. Pan, *Antioxid. Redox Signal.* **2012**, *16*, 1215-1228.
[10] a) D. Kanojia, W. Zhou, J. Zhang, C. Jie, P. K. Lo, Q. Wang, H. Chen, *Proteomics* **2012**, *12*, 3407-3415; b) K. Liao, B. Xia, Q. Y. Zhuang, M. J. Hou, Y. J. Zhang, B. Luo, Y. Qiu, Y. F. Gao, X. J. Li, H. F. Chen, W. H. Ling, C. Y. He, Y. J. Huang, Y. C. Lin, Z. N. Lin, *Theranostics* **2015**, *5*, 302-321; c) L. Y. Pang, E. A. Hurst, D. J. Argyle, *Stem Cells Int.* **2016**, *2016*, 11; d) V. Sharma, D. Dixit, S. Ghosh, E. Sen, *Neurochem. Int.* **2011**, *59*, 567-571; e) B. Singh, K. R. Cook, L. Vincent, C. S. Hall, C. Martin, A. Lucci, *J. Surg. Res.* **2011**, *168*, e39-49.
[11] J. C. Wang, *Cell Stem Cell* **2007**, *1*, 497-501.
[12] a) C. Marzano, M. Pellei, F. Tisato, C. Santini, *Anticancer Agents Med. Chem.* **2009**, *9*, 185-211; b) C. Santini, M. Pellei, V. Gandin, M. Porchia, F. Tisato, C. Marzano, *Chem. Rev.* **2014**, *114*, 815-862.

[13] a) G. B. Deacon, R. J. Phillips, *Coord. Chem. Rev.* **1980**, *33*, 227-250; b) D. Martinez, M. Motevalli, M. Watkinson, *Dalton Trans.* **2010**, *39*, 446-455.

[14] a) W.-J. Lian, X.-T. Wang, C.-Z. Xie, H. Tian, X.-Q. Song, H.-T. Pan, X. Qiao, J.-Y. Xu, *Dalton Trans.* **2016**, *45*, 9073-9087; b) X. Qiao, Z. Y. Ma, C. Z. Xie, F. Xue, Y. W. Zhang, J. Y. Xu, Z. Y. Qiang, J. S. Lou, G. J. Chen, S. P. Yan, *J. Inorg. Biochem.* **2011**, *105*, 728-737.

[15] a) D. S. Sigman, *Acc. Chem. Res.* **1986**, *19*, 180-186; b) T. B. Thederahn, M. D. Kuwabara, T. A. Larsen, D. S. Sigman, *J. Am. Chem. Soc.* **1989**, *111*, 4941-4946.

[16] a) M. A. Husain, Z. Yaseen, S. U. Rehman, T. Sarwar, M. Tabish, *FEBS J.* **2013**, *280*, 6569-6580; b) D.-D. Li, J.-L. Tian, W. Gu, X. Liu, S.-P. Yan, *Eur. J. Inorg. Chem.* **2009**, *2009*, 5036-5045.

[17] a) S. R. Smith, G. A. Neyhart, W. A. Kalsbeck, H. H. Thorp, *New J. Chem.* **1994**, *18*, 397-406; b) A. Wolfe, G. H. Shimer, T. Meehan, *Biochemistry* **1987**, *26*, 6392-6396.

[18] B. M. Zeglis, V. C. Pierre, J. K. Barton, *Chem. Commun.* **2007**, 4565-4579.

[19] A. A. Kumbhar, A. T. Franks, R. J. Butcher, K. J. Franz, *Chem. Commun.* **2013**, *49*, 2460-2462.

[20] P. B. Gupta, T. T. Onder, G. Jiang, K. Tao, C. Kuperwasser, R. A. Weinberg, E. S. Lander, *Cell* **2009**, *138*, 645-659.

[21] G. Dontu, W. M. Abdallah, J. M. Foley, K. W. Jackson, M. F. Clarke, M. J. Kawamura, M. S. Wicha, *Genes Dev.* **2003**, *17*, 1253-1270.

[22] I. Morita, M. Schindler, M. K. Regier, J. C. Otto, T. Hori, D. L. DeWitt, W. L. Smith, *J. Biol. Chem.* **1995**, *270*, 10902-10908.

[23] M. J. Chow, C. Licona, G. Pastorin, G. Mellitzer, W. H. Ang, C. Gaiddon, *Chem. Sci.* **2016**, *7*, 4117-4124.

[24] a) J. Y. Ahn, J. K. Schwarz, H. Piwnica-Worms, C. E. Canman, *Cancer Res.* **2000**, *60*, 5934-5936; b) S. Burma, B. P. Chen, M. Murphy, A. Kurimasa, D. J. Chen, *J. Biol. Chem.* **2001**, *276*, 42462-42467; c) S. Matsuoka, G. Rotman, A. Ogawa, Y. Shiloh, K. Tamai, S. J. Elledge, *Proc. Natl. Acad. Sci. U.S.A.* **2000**, *97*, 10389-10394; d) R. Melchionna, X. B. Chen, A. Blasina, C. H. McGowan, *Nature Cell Biol.* **2000**, *2*, 762-765; e) E. P. Rogakou, D. R. Pilch, A. H. Orr, V. S. Ivanova, W. M. Bonner, *J. Biol. Chem.* **1998**, *273*, 5858-5868.

[25] W. P. Roos, A. D. Thomas, B. Kaina, *Nat. Rev. Cancer* **2016**, *16*, 20-33.

[26] A. Nassar, A. Radhakrishnan, I. A. Cabrero, G. Cotsonis, C. Cohen, *Appl. Immunohistochem. Mol. Morphol.* **2007**, *15*, 255-259.

[27] B. Singh, J. A. Berry, A. Shoher, V. Ramakrishnan, A. Lucci, *Int. J. Oncol.* **2005**, *26*, 1393-1399.

Entry for the Table of Contents (Please choose one layout)

Layout 1:

FULL PAPER

Text for Table of Contents

Two birds with one copper stone: We present a series of copper(II) complexes containing vanillin Schiff base derivatives and the nonsteroidal anti-inflammatory drug, naproxen. Three of the complexes kill bulk cancer cells and cancer stem cells with similar doses. The most effective complex evokes cell death by inducing DNA damage and inhibiting cyclooxygenase-2.

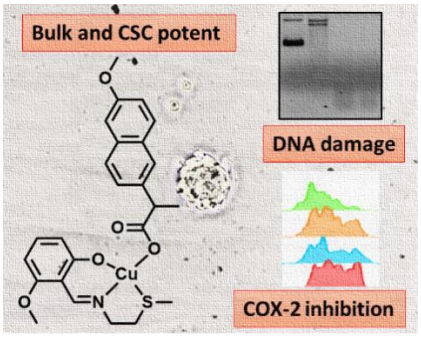

*Author(s), Corresponding Author(s)**

Page No. – Page No.

Title

Supporting Information

Table of Content

Table S2. IC_{50} values of the copper(II) complexes, **1**-**4** against GM05757 cells. Determined after 72 h incubation (mean of three independent experiments ± SD).

Figure S25. Copper content in HMLER-shEcad cells treated with **1**-**4** (10 μM for 24 h).

Figure S26. Normalised ROS activity in untreated HMLER-shEcad cells (control) and HMLER-shEcad cells treated with **4** (50 μM for 6, 12, and 24 h) and co-treated with **4** (50 μM for 6, 12, and 24 h) and *N*-acetylcysteine (2.5 mM for 6, 12, and 24 h). Error bars represent standard deviations and Student *t test*, * = $p < 0.05$.

Figure S27. Normalised ROS activity in untreated HMLER-shEcad cells (control) and HMLER-shEcad cells treated with H_2O_2 (150 μM for 6, 12, and 24 h) and co-treated with H_2O_2 (150 μM for 6, 12, and 24 h) and *N*-acetylcysteine (2.5 mM for 6, 12, and 24 h). Error bars represent standard deviations and Student *t test*, ** = $p < 0.01$.

Figure S28. Immunoblotting analysis of proteins related to the DNA damage and apoptosis pathways. Protein expression in HMLER-shEcad cells following treatment with **4** (5, 10, and 20 μM) after 72 h incubation. Whole cell lysates were resolved by SDS-PAGE and analyzed by immunoblotting against γH2AX, phos-CHK2, cleaved caspase 7, cleaved caspase 3, and β-actin (loading control).

Figure S29. Representative histograms displaying the green fluorescence emitted by anti-COX-2 Alexa Fluor 488 nm antibody-stained HMLER-shEcad cells treated with LPS (2.5 μM) for 24 h (red) followed by 48 h in media containing naproxen (20 μM, blue).

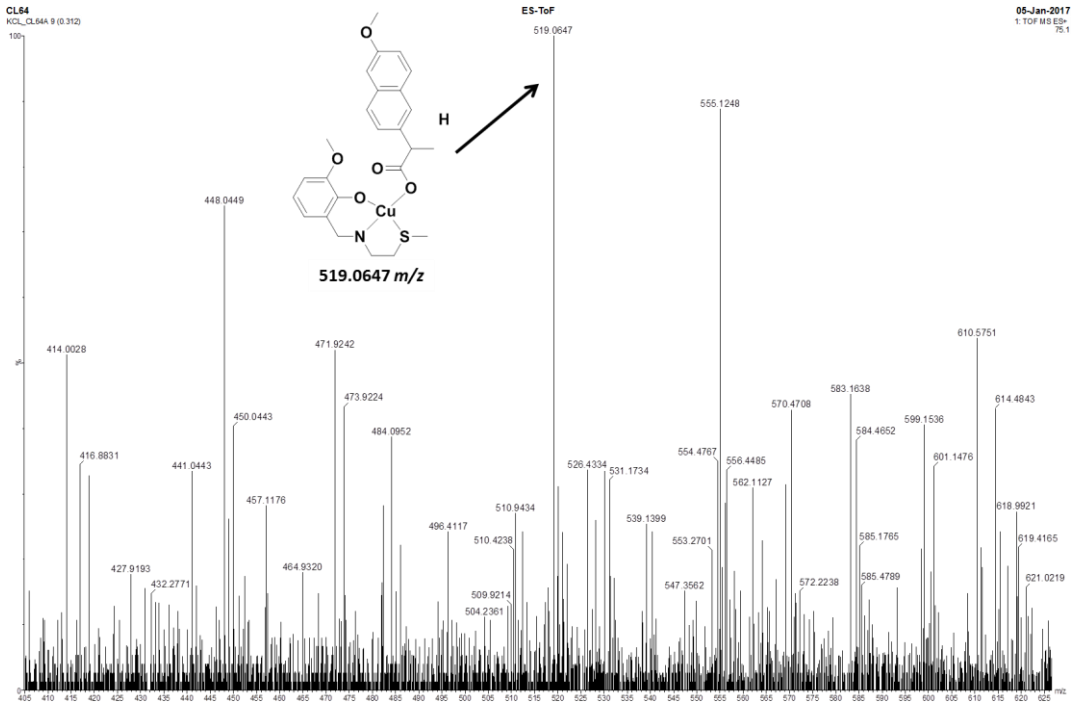

Figure S1. High resolution ESI-TOF mass spectrum (positive mode) of **1**.

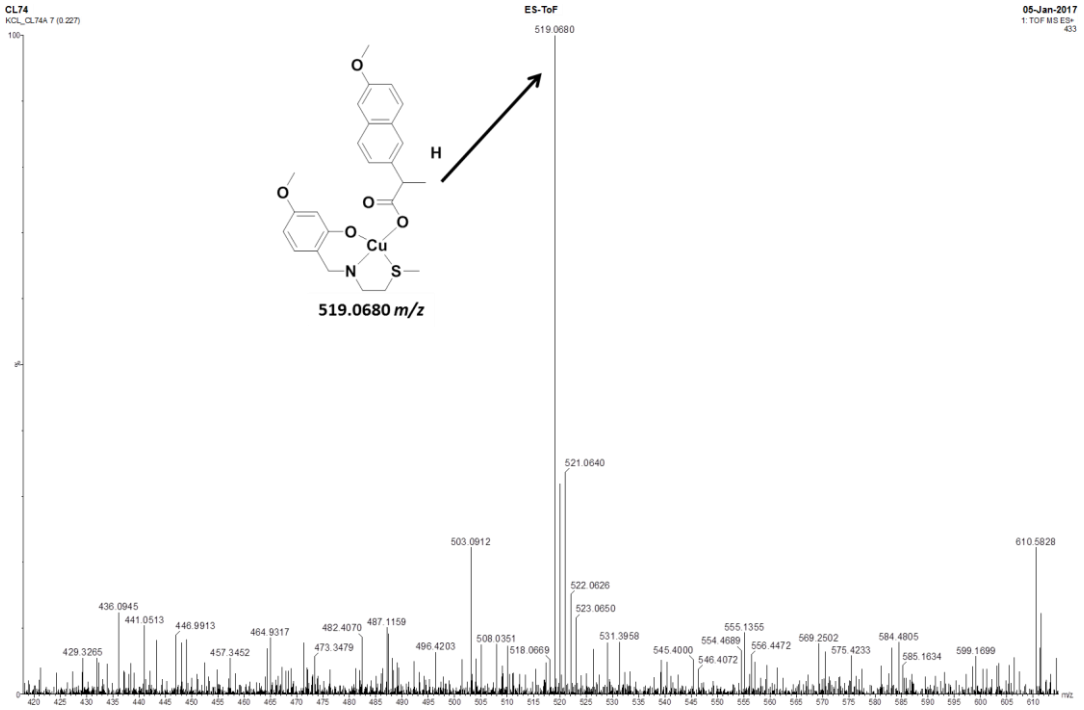

Figure S2. High resolution ESI-TOF mass spectrum (positive mode) of **2**.

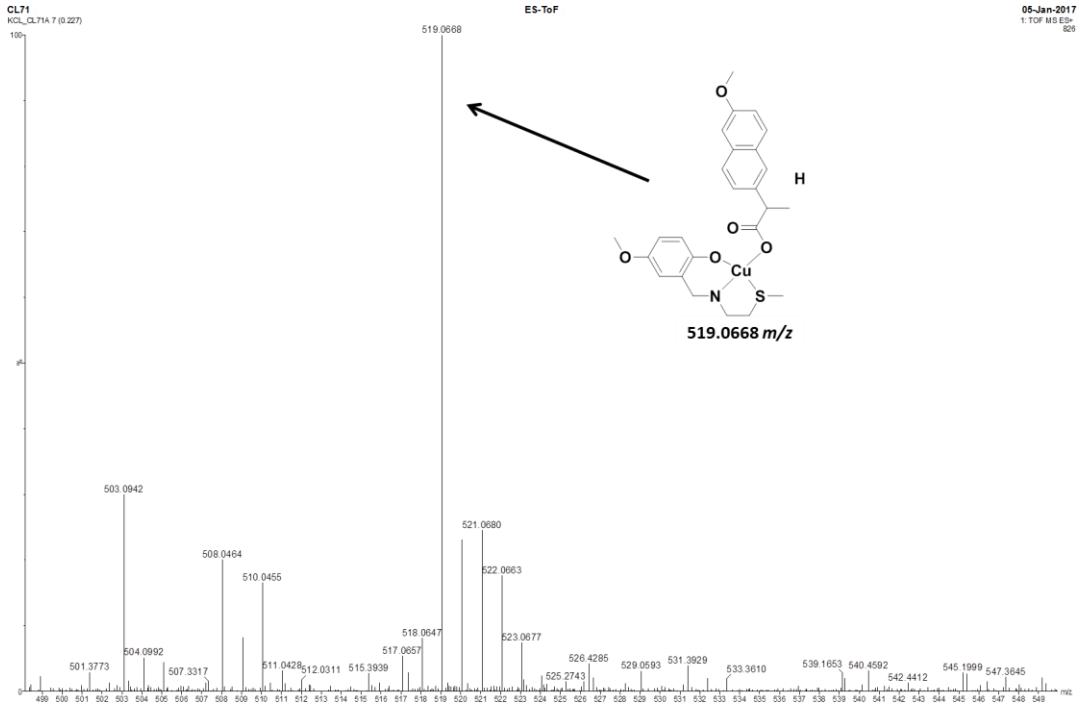

Figure S3. High resolution ESI-TOF mass spectrum (positive mode) of **3**.

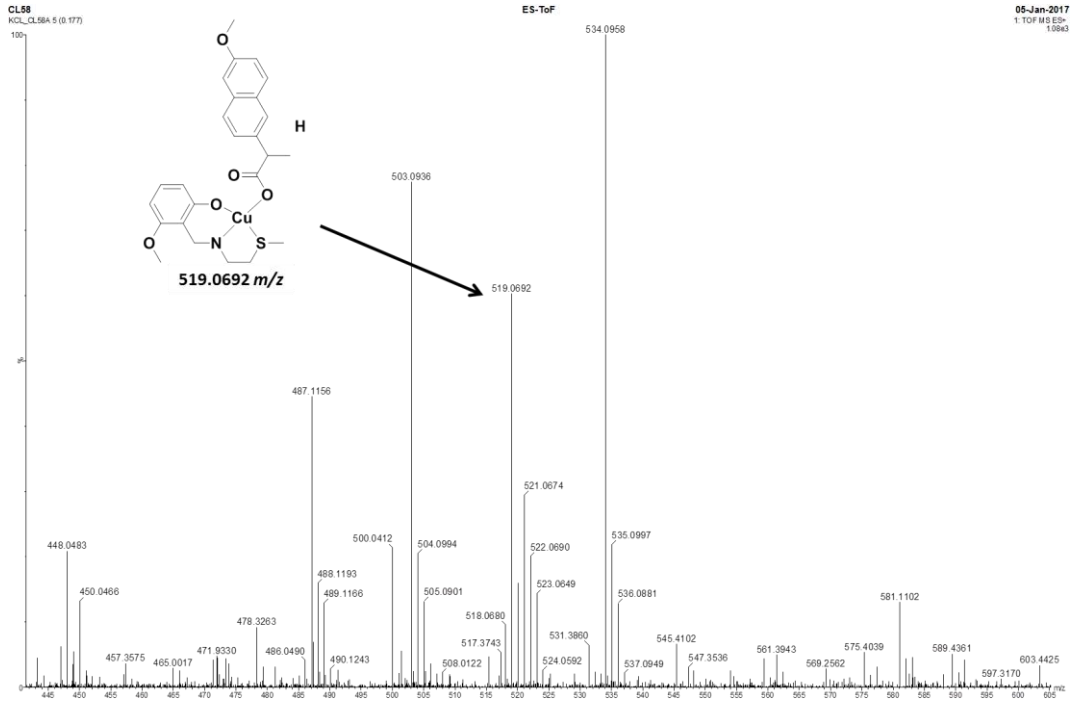

Figure S4. High resolution ESI-TOF mass spectrum (positive mode) of **4**.

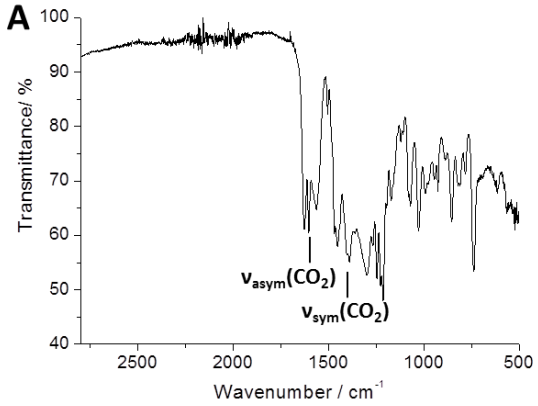

IR (solid, cm^{-1}): 1627, 1603, 1563, 1469, 1453, 1390, 1301, 1247, 1227, 1214, 1171, 1071, 1029, 927, 855, 780, 739.

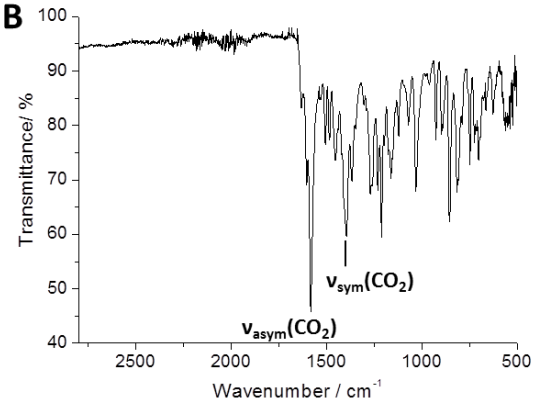

IR (solid, cm^{-1}): 1606, 1583, 1506, 1483, 1454, 1397, 1367, 1271, 1232, 1212, 1163, 1033, 928, 899, 855, 817, 749, 704.

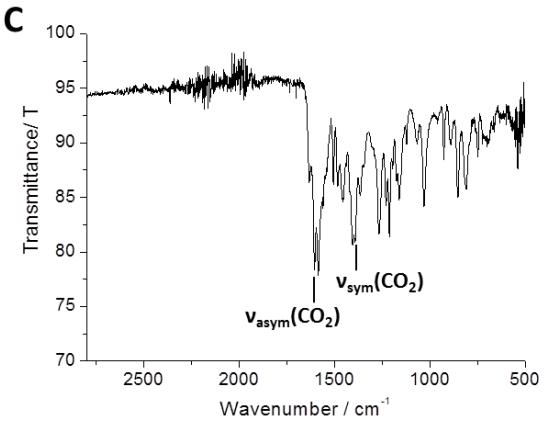

IR (solid, cm^{-1}): 1633, 1604, 1585, 1506, 1483, 1457, 1406, 1393, 1366, 1268, 1229, 1213, 1161, 1032, 928, 853, 809, 749.

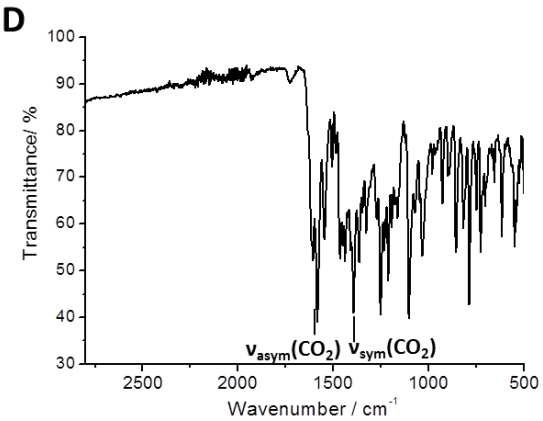

IR (solid, cm^{-1}): 1607, 1585, 1548, 1396, 1363, 1252, 1212, 1105, 1034, 927, 856, 818, 788, 750, 729, 616, 548.

Figure S5. IR spectrum of (A) **1**, (B) **2**, (C) **3**, and (D) **4** in the solid form.

Figure S6. Concentration-dependent DNA cleavage by **1**-**3** after a 24 h incubation period. a) Lane 1: DNA only; Lane 2-4: DNA + 10, 25, and 50 µM of **1**; b) Lane 1: DNA only; Lane 2-4: DNA + 10, 25, and 50 µM of **2**; c) Lane 1: DNA only; Lane 2-4: DNA + 10, 25, and 50 µM of **3**.

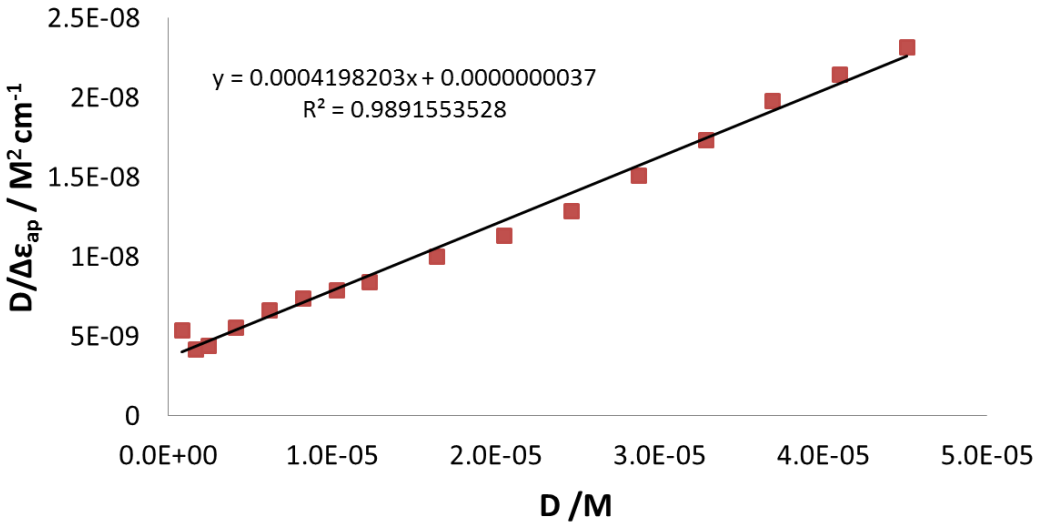

Figure S7. Representative reciprocal plot of $D/\Delta\varepsilon_{ap}$ versus D of **4** (50µM) upon addition of ct-DNA (0 – 0.9 eq.).

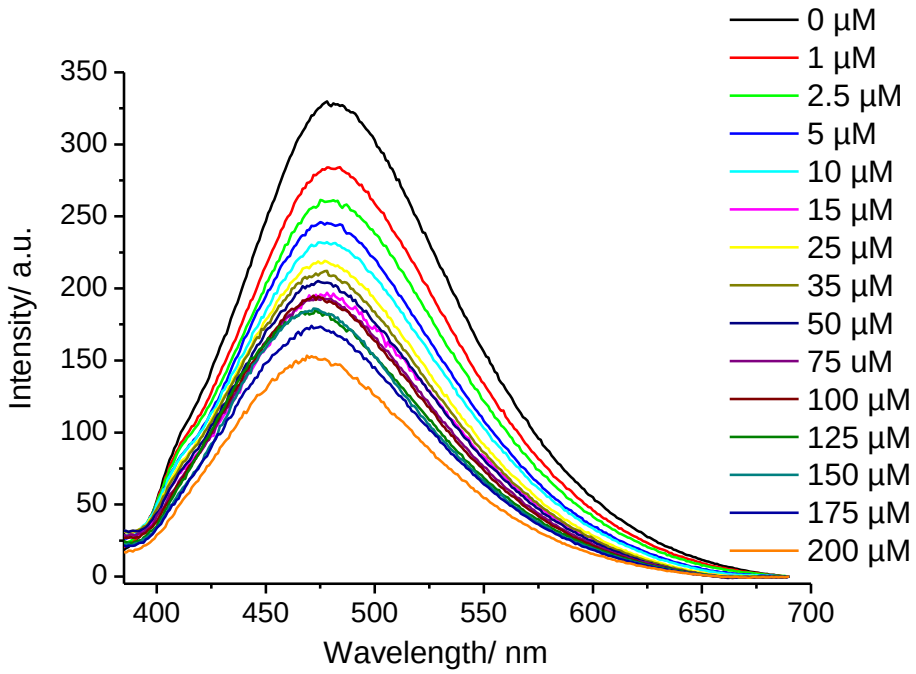

Figure S8. Emission spectra for DAPI (1 µM) bound to ct-DNA (20 µM) upon addition of aliquots of **4** (0-200 µM).

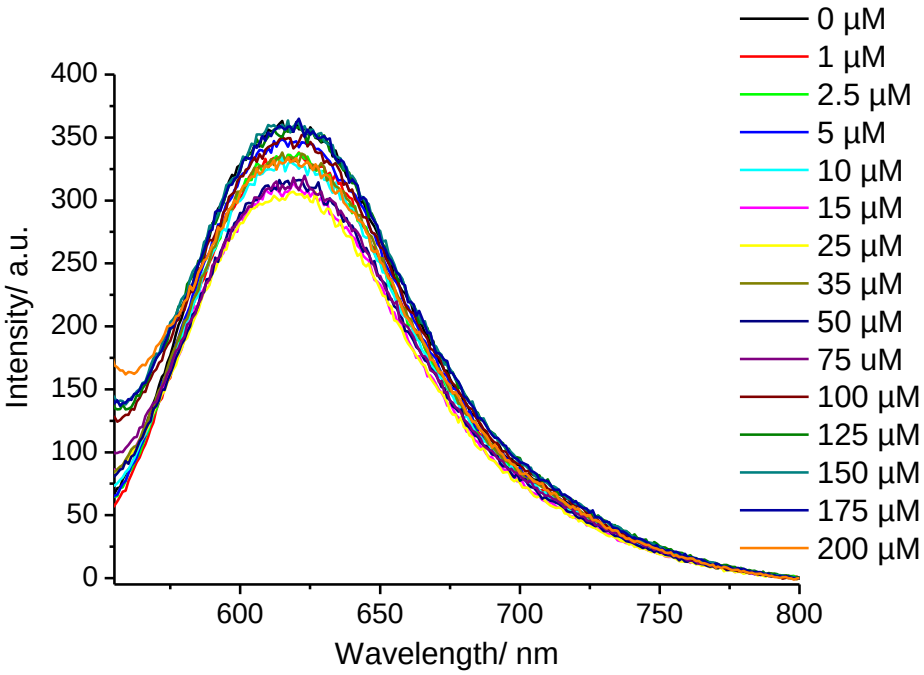

Figure S9. Emission spectra for ethidium bromide (1 µM) bound to ct-DNA (20 µM) upon addition of aliquots of **4** (0-200 µM).

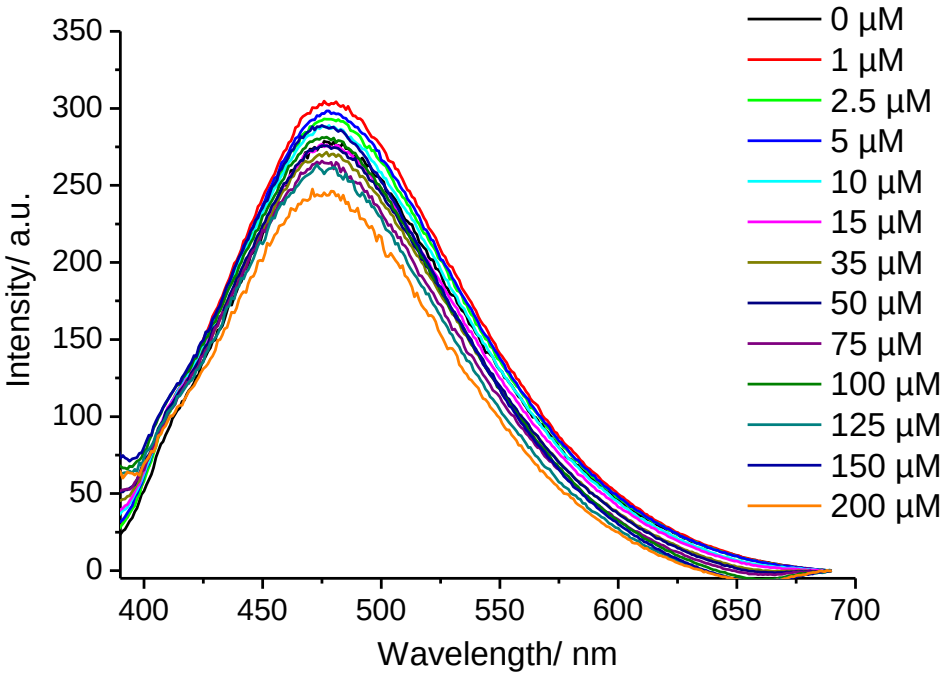

Figure S10. Emission spectra for DAPI (1 µM) bound to ct-DNA (20 µM) upon addition of aliquots of naproxen (0-200 µM).

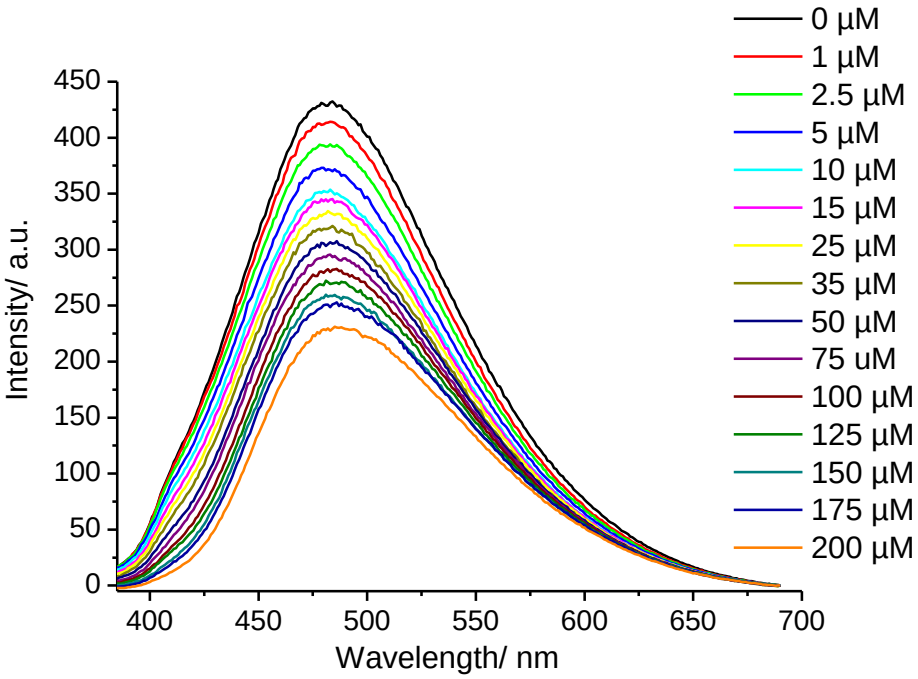

Figure S11. Emission spectra for DAPI (1 µM) bound to ct-DNA (20 µM) upon addition of aliquots of **L**^{4} (0-200 µM).

Table S1. Experimentally determined LogP values for **1**-**4** (mean of three independent experiments ± SD).

Cu(II) complex	LogP
1	-0.171 ± 0.032
2	-0.200 ± 0.011
3	-0.102 ± 0.077
4	-0.093 ± 0.015

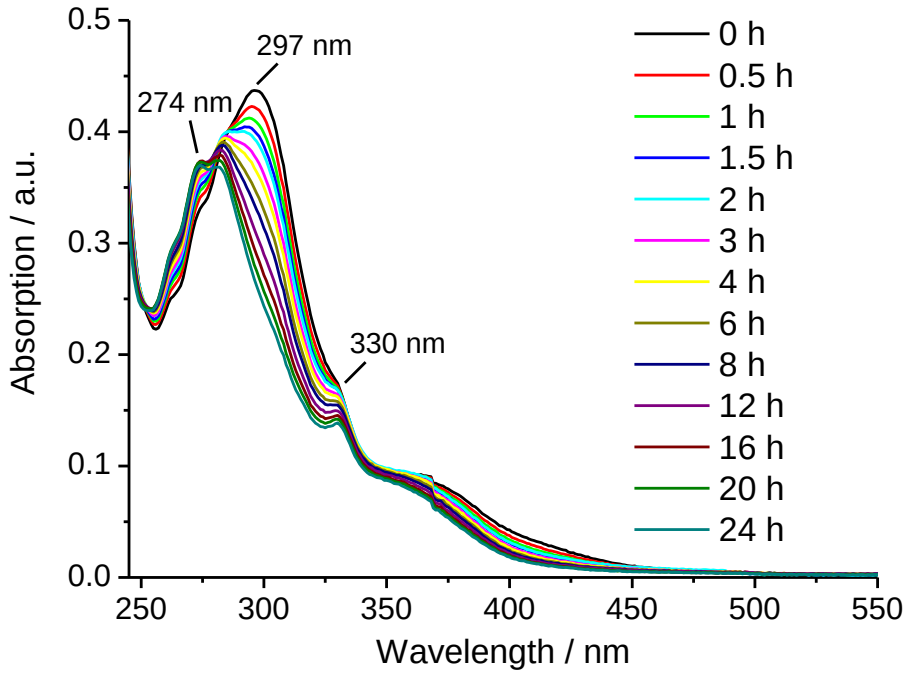

Figure S12. UV-Vis spectrum of **4** (50 μM) in PBS over the course of 24 h at 37 ºC.

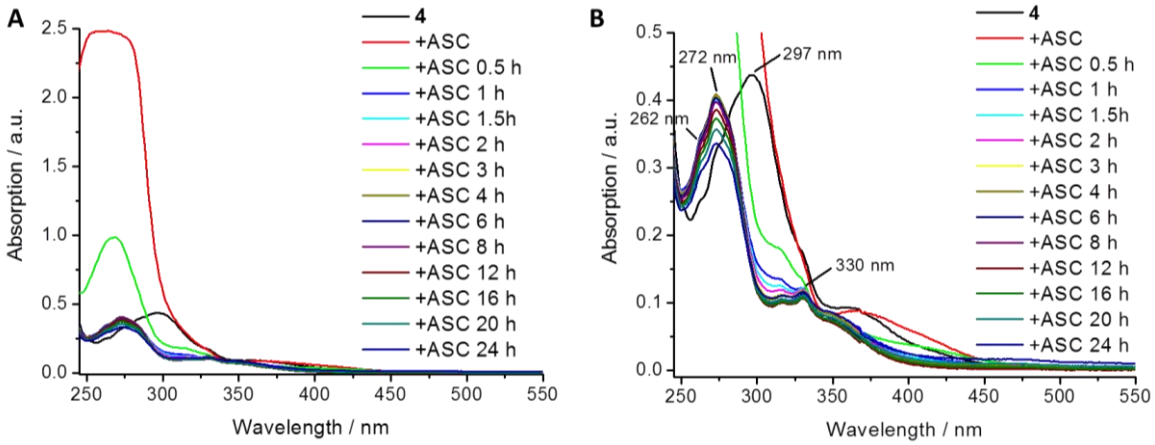

Figure S13. UV-Vis spectrum of **4** (50 μM) in the presence of ascorbic acid (500 μM) in PBS over the course of 24 h at 37 ºC. (A) Absorption intensity is shown from 0 - 2.5 a.u. and (B) from 0 - 0.5 a.u for clarity.

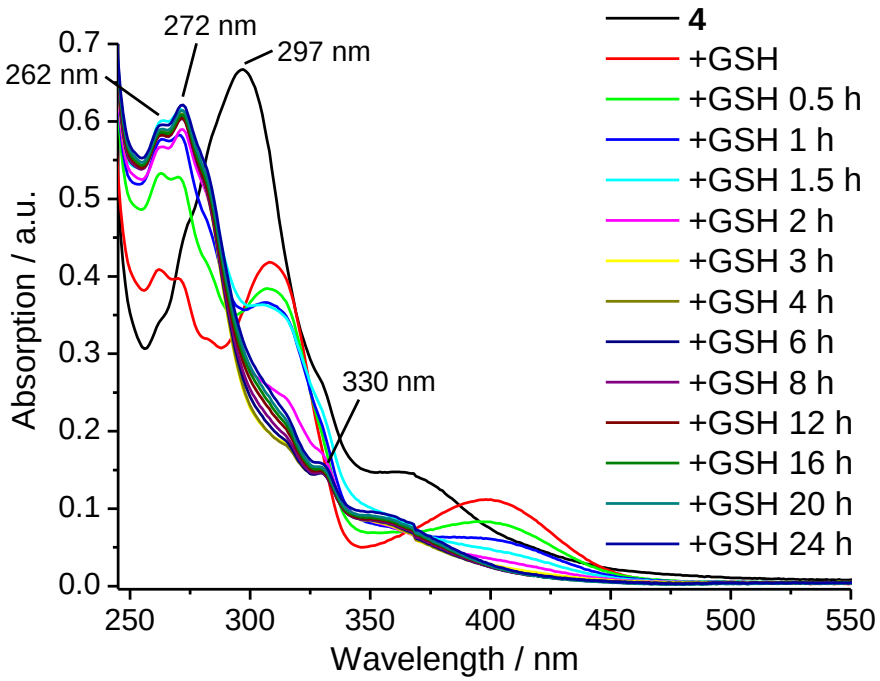

Figure S14. UV-Vis spectrum of **4** (50 μM) in the presence of glutathione (500 μM) in PBS over the course of 24 h at 37 ºC.

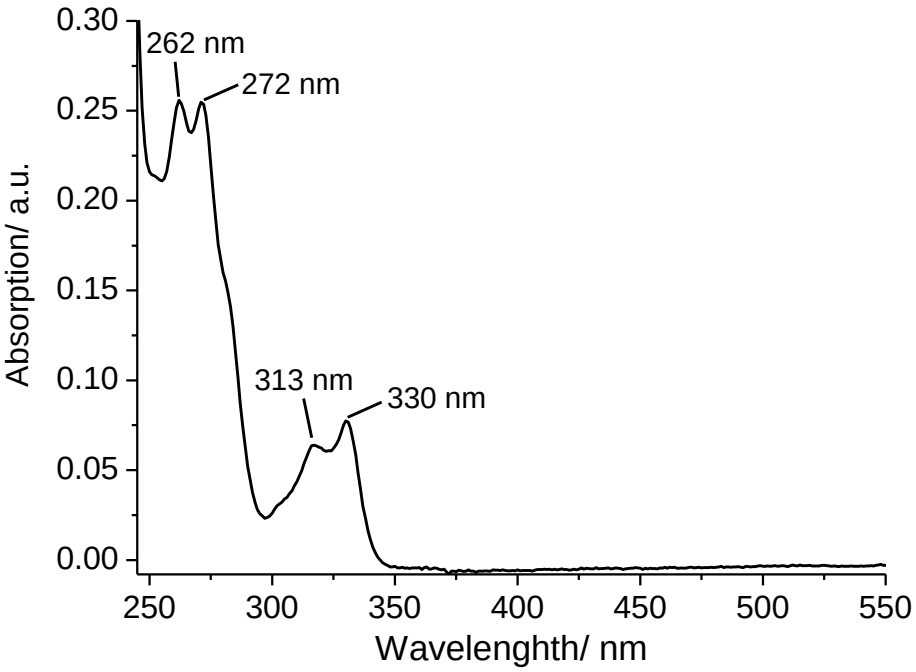

Figure S15. UV-vis spectrum of naproxen (50 μM) in PBS at 37 ºC.

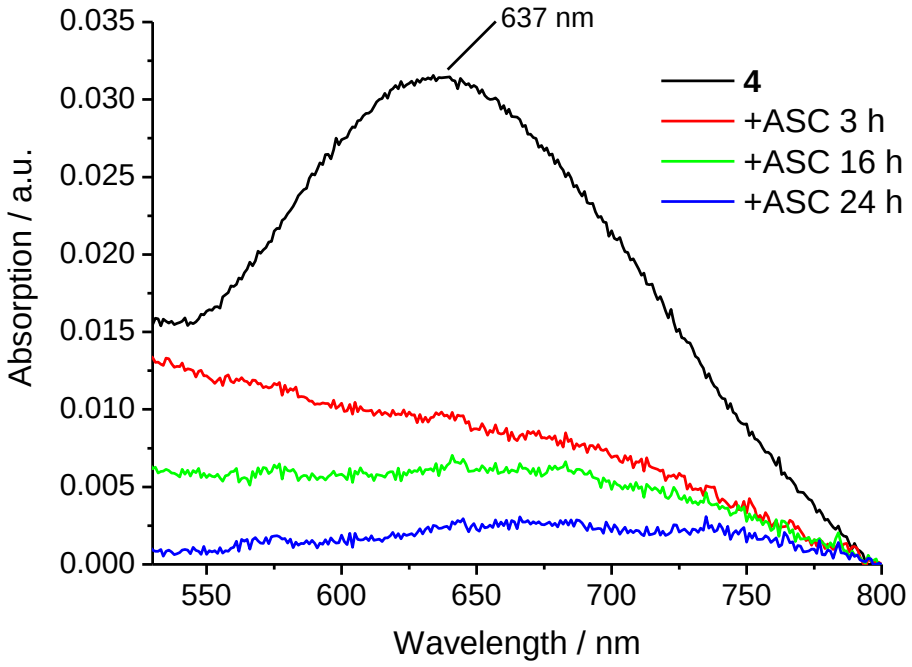

Figure S16. UV-Vis spectrum of **4** (250 μM) in the presence of ascorbic acid (2.5 mM) in PBS:DMSO (99:1) over the course of 24 h at 37 ºC.

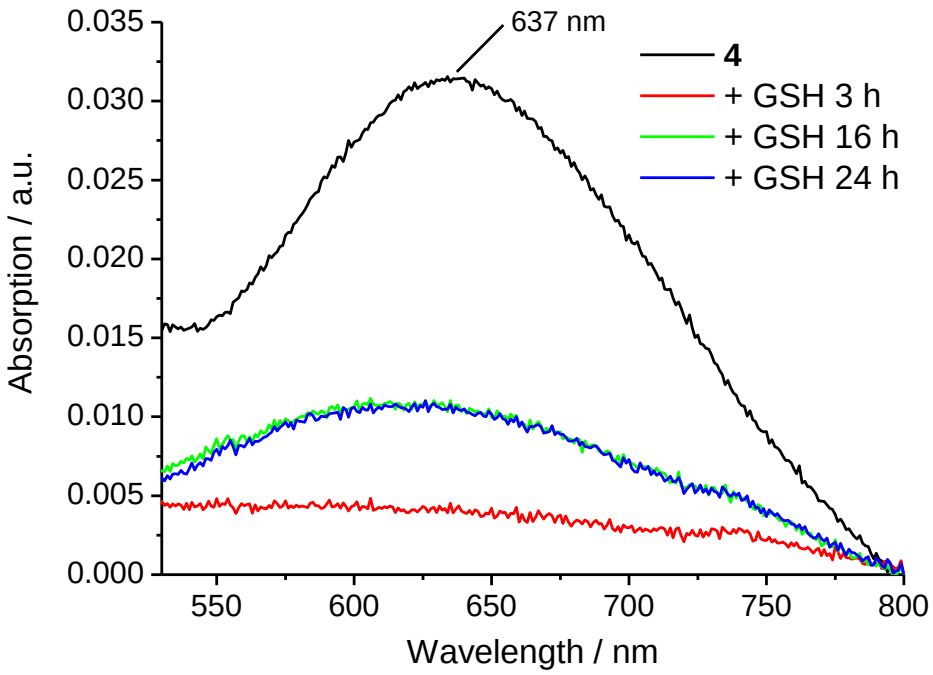

Figure S17. UV-Vis spectrum of **4** (250 μM) in the presence of glutathione (2.5 mM) in PBS:DMSO (99:1) over the course of 24 h at 37 ºC.

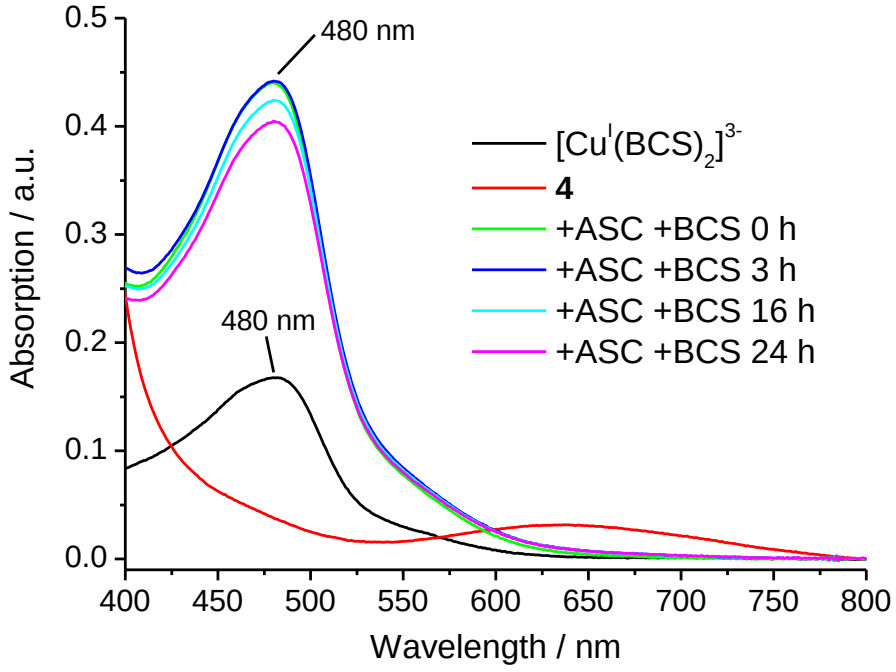

Figure S18. UV-Vis spectrum of **4** (50 μM) in the presence of ascorbic acid (500 μM) and bathocuproine disulfonate, BCS (100 μM) in PBS over the course of 24 h at 37 ºC.

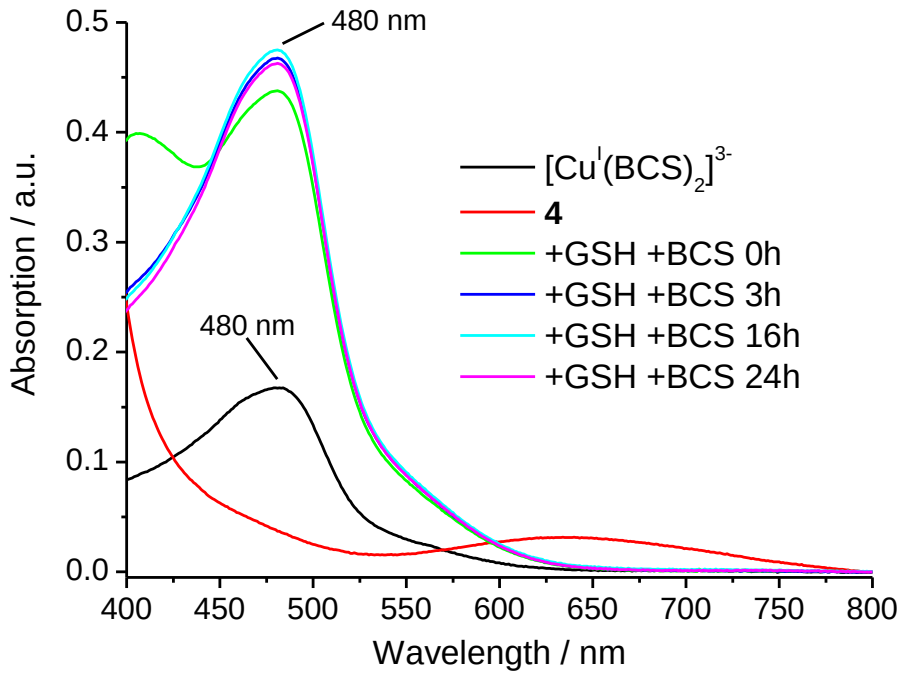

Figure S19. UV-Vis spectrum of **4** (50 μM) in the presence of glutathione (500 μM) and bathocuproine disulfonate, BCS (100 μM) in PBS over the course of 24 h at 37 ºC.

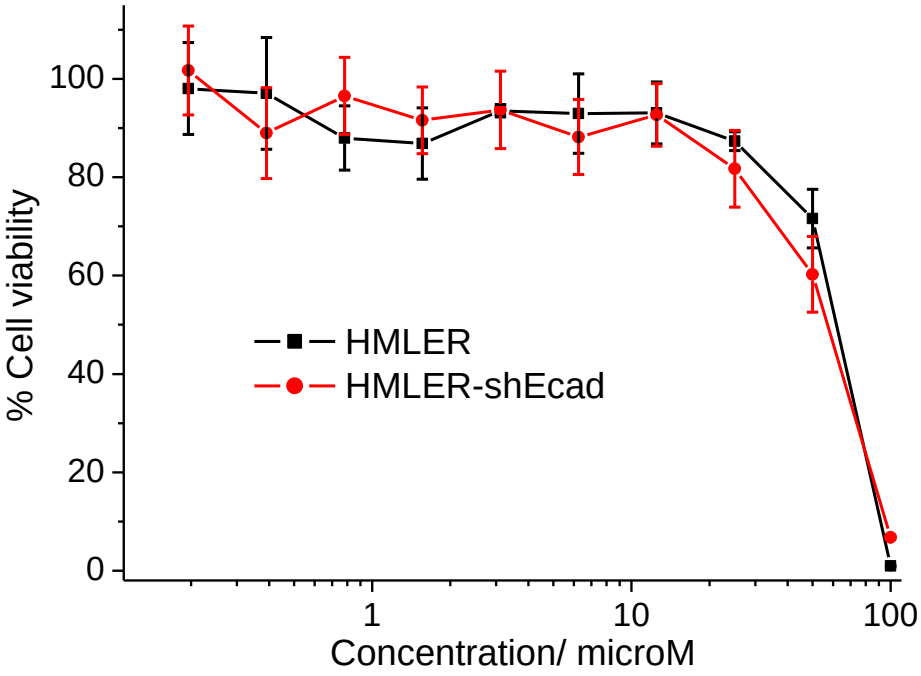

Figure S20. Representative dose-response curves for the treatment of HMLER and HMLER-shEcad cells with **1** after 72 h incubation.

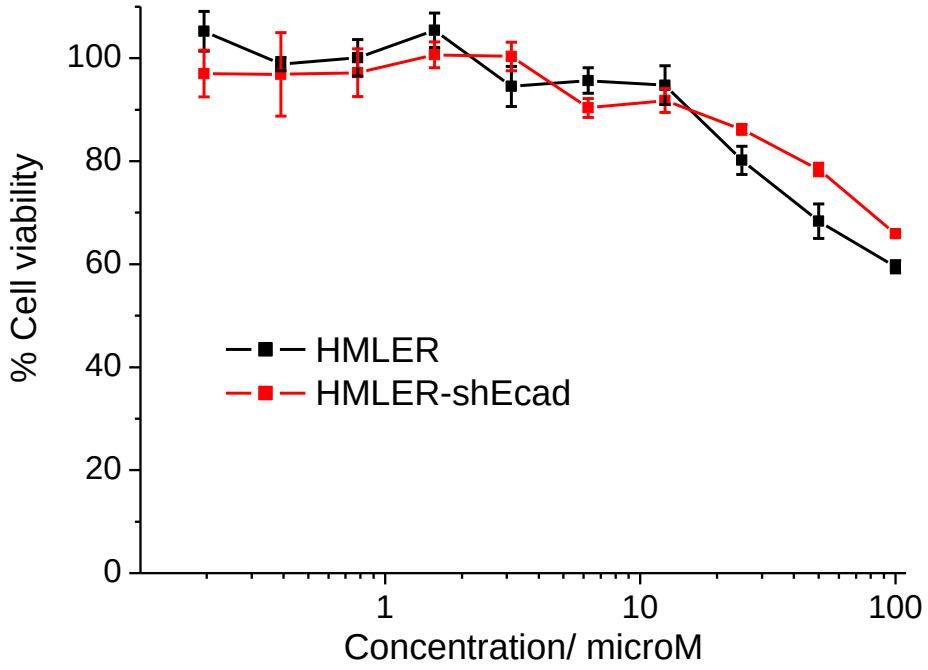

Figure S21. Representative dose-response curves for the treatment of HMLER and HMLER-shEcad cells with **2** after 72 h incubation.

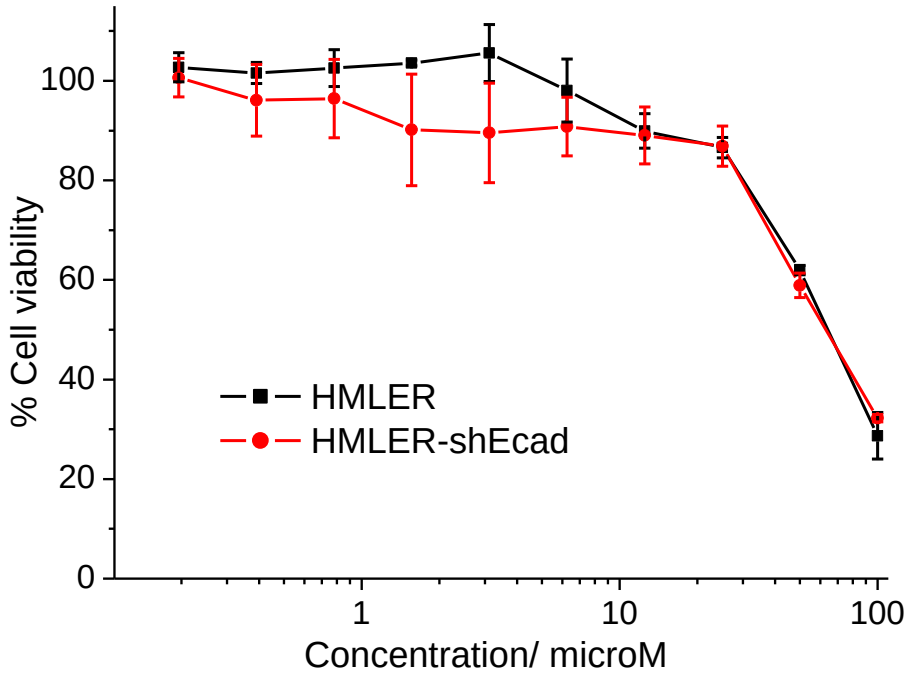

Figure S22. Representative dose-response curves for the treatment of HMLER and HMLER-shEcad cells with **3** after 72 h incubation.

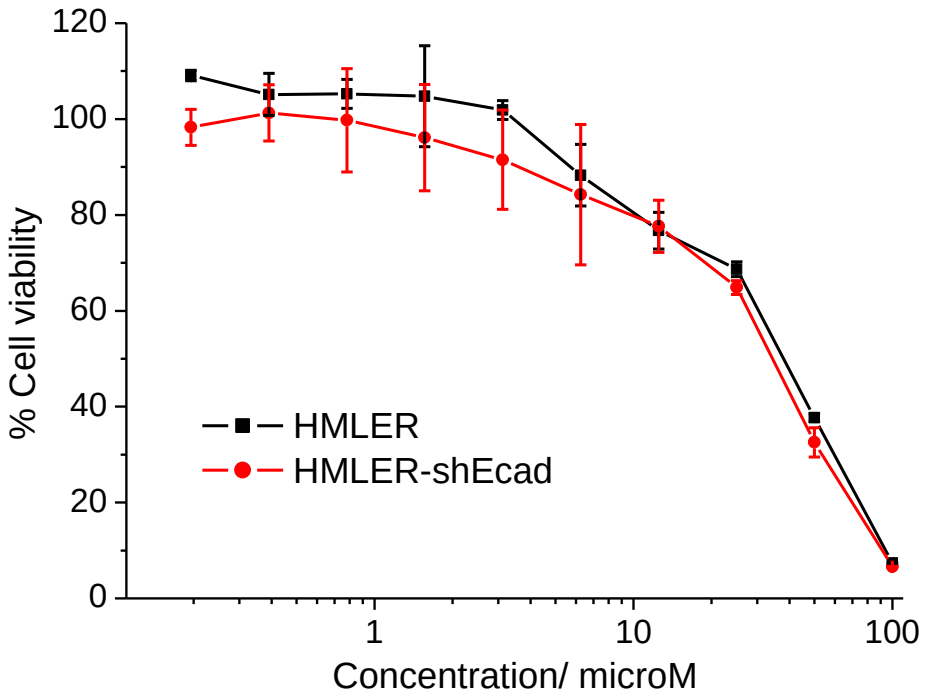

Figure S23. Representative dose-response curves for the treatment of HMLER and HMLER-shEcad cells with **4** after 72 h incubation.

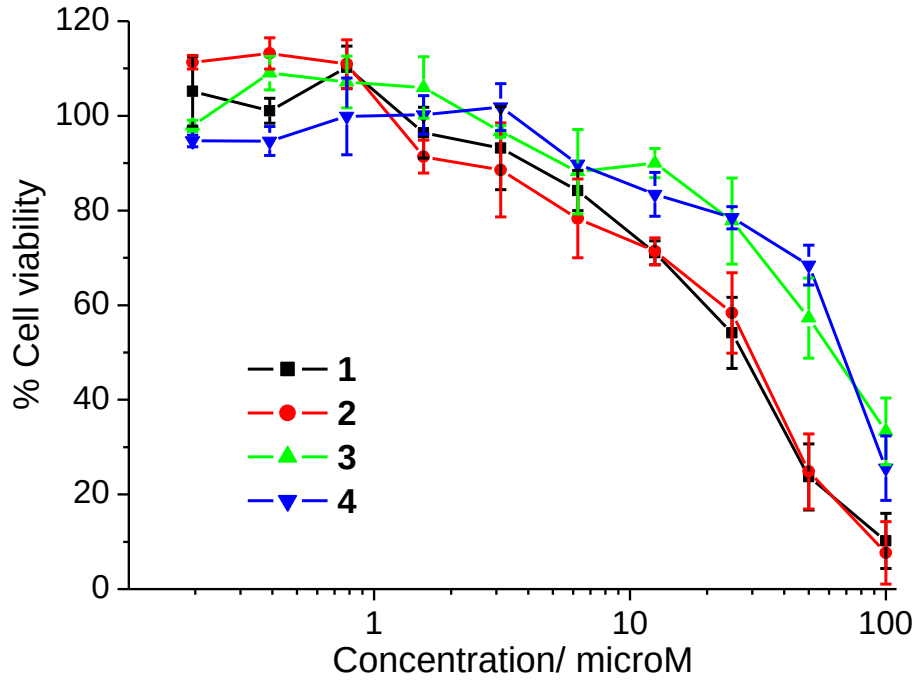

Figure S24. Representative dose-response curves for the treatment of GM05757 cells with **1**-**4** after 72 h incubation.

Table S2. IC_{50} values of the copper(II) complexes, **1**-**4** against GM05757 cells. Determined after 72 h incubation (mean of three independent experiments ± SD).

Cu(II) complex	GMO5757 IC_{50} [μM]
1	29.7 ± 2.9
2	33.8 ± 4.7
3	62.6 ± 0.6
4	71.1 ± 1.1

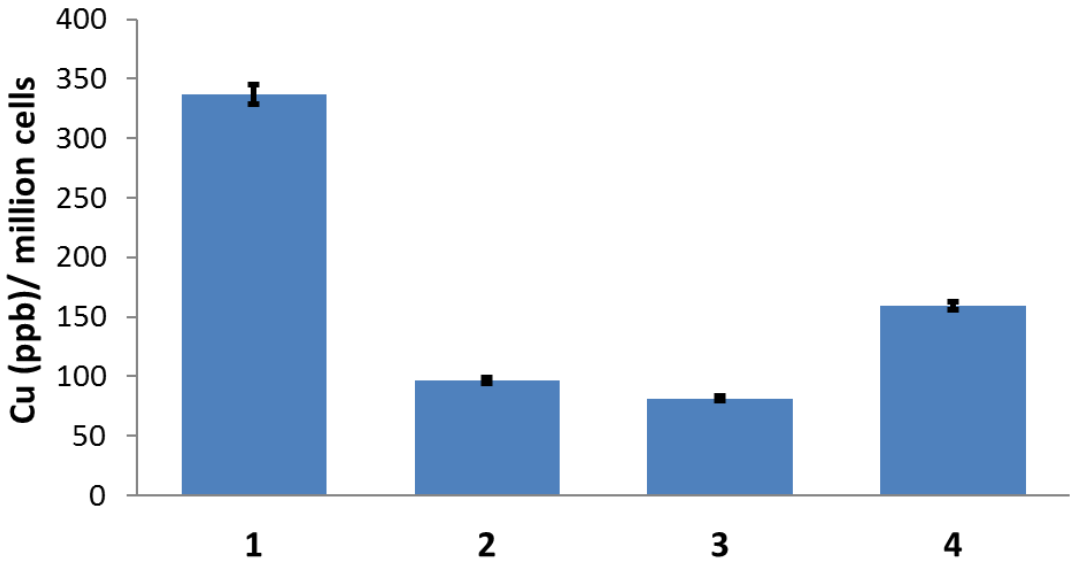

Figure S25. Copper content in HMLER-shEcad cells treated with **1**-**4** (10 μM for 24 h).

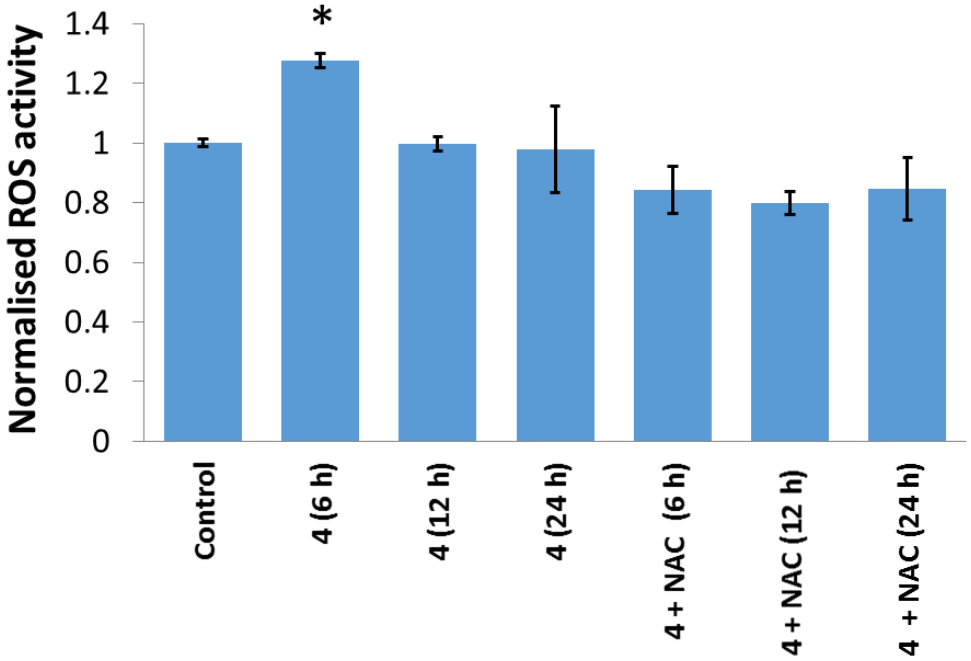

Figure S26. Normalised ROS activity in untreated HMLER-shEcad cells (control) and HMLER-shEcad cells treated with **4** (50 µM for 6, 12, and 24 h) and co-treated with **4** (50 µM for 6, 12, and 24 h) and *N*-acetylcysteine (2.5 mM for 6, 12, and 24 h). Error bars represent standard deviations and Student *t test*, * = $p < 0.05$.

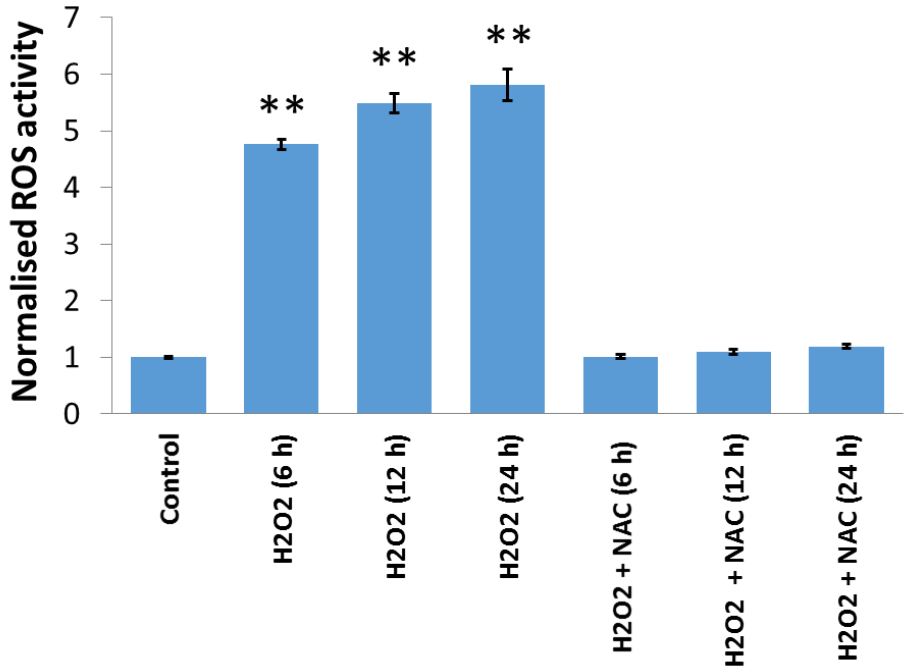

Figure S27. Normalised ROS activity in untreated HMLER-shEcad cells (control) and HMLER-shEcad cells treated with H_2O_2 (150 µM for 6, 12, and 24 h) and co-treated with H_2O_2 (150 µM for 6, 12, and 24 h) and *N*-acetylcysteine (2.5 mM for 6, 12, and 24 h). Error bars represent standard deviations and Student *t test*, ** = $p < 0.01$.

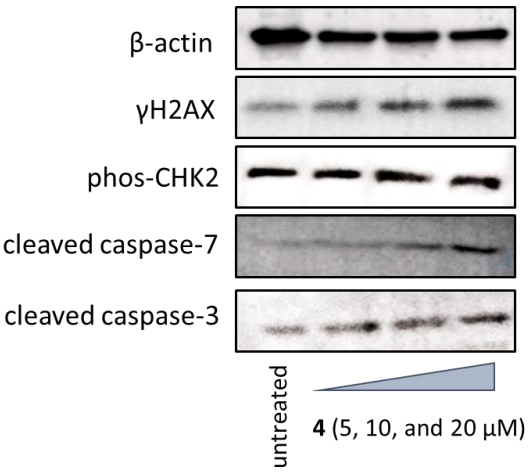

Figure S28. Immunoblotting analysis of proteins related to the DNA damage and apoptosis pathways. Protein expression in HMLER-shEcad cells following treatment with **4** (5, 10, and 20 μM) after 72 h incubation. Whole cell lysates were resolved by SDS-PAGE and analyzed by immunoblotting against γH2AX, phos-CHK2, cleaved caspase 7, cleaved caspase 3, and β-actin (loading control).

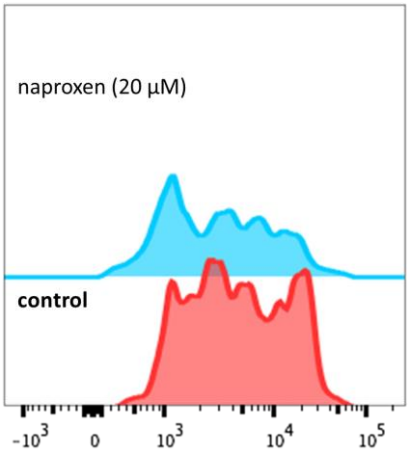

Figure S29. Representative histograms displaying the green fluorescence emitted by anti-COX-2 Alexa Fluor 488 nm antibody-stained HMLER-shEcad cells treated with LPS (2.5 μM) for 24 h (red) followed by 48 h in media containing naproxen (20 μM, blue).